Mechanics of Advanced Materials and Structures

ISSN: (Print) (Online) Journal homepage: https://www.tandfonline.com/loi/umcm20

# Exact strain gradient modelling of prestressed nonlocal diatomic lattice metamaterials

Binying Wang, Jinxing Liu, Ai Kah Soh & Naigang Liang

**To cite this article:** Binying Wang, Jinxing Liu, Ai Kah Soh & Naigang Liang (2022): Exact strain gradient modelling of prestressed nonlocal diatomic lattice metamaterials, Mechanics of Advanced Materials and Structures, DOI: 10.1080/15376494.2022.2062629

**To link to this article:** https://doi.org/10.1080/15376494.2022.2062629

Published online: 28 Apr 2022.

MECHANICS OF ADVANCED MATERIALS AND STRUCTURES
https://doi.org/10.1080/15376494.2022.2062629

Taylor & Francis
Taylor & Francis Group

Check for updates

ORIGINAL ARTICLE

# Exact strain gradient modelling of prestressed nonlocal diatomic lattice metamaterials

Binying Wang[a], Jinxing Liu[a], Ai Kah Soh[b], and Naigang Liang[c]

[a]Faculty of Civil Engineering and Mechanics, Jiangsu University, Zhenjiang, PR China; [b]School of Engineering, Monash University Malaysia, Jalan Lagoon Selatan, Selangor Darul Ehsan, Bandar Sunway, Malaysia; [c]Institute of Mechanics, Chinese Academy of Sciences, Beijing, PR China

**ABSTRACT**

In this article, an exact strain gradient (SG) continuum model to capture the broadband bandgap characteristics of the prestressed diatomic lattice (PDL) with local/nonlocal interactions has been proposed. By considering the periodicity of wave motion, the wavelength-dependent Taylor expansion is established, leading to a desirable prediction when the wavelength is close to the lattice scale. For PDL, the dispersion curves of the proposed continuum model are always consistent with those of discrete model in the first Brillouin zone. The proposed SG continuum model is used to investigate the effects of structural parameters, orders of SG continua and various nonlocal interactions on bandgap properties of PDL.

**ARTICLE HISTORY**
Received 18 January 2022
Accepted 2 April 2022

**KEYWORDS**
Band gap; strain gradient continuum; dispersion; Brillouin zone; nonlocal interaction; prestress; Taylor expansion

**HIGHLIGHTS**

- Continuum modelling of prestressed acoustic diatomic lattices.
- Perfect agreements achieved between dispersion diagrams by discrete and proposed continuum models.
- Effects of prestress, nonlocal interactions, mass and stiffness ratios on band gap structures analyzed.
- Proper strain gradient (SG) orders determined to guarantee a satisfactory accuracy.

## 1. Introduction

In recent decades, efforts have been devoted to researches of metamaterials to promote both lattice metamaterial theory and technology development. Metamaterials refer to a new kind of artificially synthetic materials, which possess some novel properties not found in conventional materials [1, 2]. In such a context, acoustic metamaterials can exhibit unique physical characteristics, such as effective negative bulk modulus, effective negative mass density, etc. These extraordinary properties also make acoustic metamaterials achieve great progress in practical application including noise control, vibration suppression, waveguides, invisible cloaks and so on [3, 4]. Particularly, many researches have been carried out to analyze the wave propagation, dispersion characteristics and effective negative parameters in elastic metamaterials [5–12].

One of the most attractive advantages of metamaterials is their ability to prevent elastic wave to propagate within certain frequency ranges, i.e., the so-called bandgaps. There are two physical formation mechanisms for bandgaps [13]. One is Bragg scattering, meaning that bandgaps are generated due to the multiple scattering of periodic structures, when the wavelength is close to lattice size. The other is local resonance, signifying that these bandgaps formation relies on the vibration of local resonators and appear around the resonant frequency [14]. Therefore, metamaterials with local resonators can be built to create low-frequency band gaps, which are suitable for vibration isolation and noise reduction. However, the narrower band widths often limit the applicability of them. In the past few decades, many relevant studies have been conducted to increase the band width and adjust the band gap distribution. To achieve multiple and wider bandgaps for broadband vibration suppression, Hu et al. [15] and Zhao et al. [16] proposed the modified metamaterials with coupled resonators and discussed band gap behavior of them based on the corresponding discrete lattice model. Tan et al. [17] provided a dual resonator microstructure design for acoustic metamaterials, achieving broadband effective mass negativity and showing the advantage of wave attenuation in a larger frequency range. In addition, the effects of complex structure configuration [18], relevant structural parameters [19] and hierarchical designs [20] on bandgaps structure of periodic lattice metamaterials have been analyzed in detail. These studies can provide a reliable guidance for the adjustment and design of bandgaps.

CONTACT Jinxing Liu jxliu@mails.ucas.ac.cn Faculty of Civil Engineering and Mechanics, Jiangsu University, Xuefu Road 301, Zhenjiang, Jiangsu Province, PR China.

As a benchmark problem, dispersion of the 1D periodic lattice has aroused increasing research interests. We can take the periodic lattice as discrete structures, and derive the equations of motion and the corresponding dispersion relations, just as done by Zhao, Zhang, Zhao and Deng [16] and Li et al. [18]. However, when we study a periodic finite lattice, which consists of numerous masses with boundary conditions particularly prescribed, the discrete model becomes too cumbersome and the continuum model tends to be a better option. A proper continuum model for 1D periodic mass-spring structure is a necessity. When the dispersive behavior of 1D periodic mass-spring structure is investigated, besides the discrete model, the equivalent continuum model with microstructure can also be established. The application of microstructure elasticity theory is easy to be limited due to the existence of too many motion freedom and material parameters. As a comparison, more attention has been focused on the gradient elastic theory with less material parameters [21]. Mindlin [22] proposed early the strain gradient (SG) elastic theories to illustrate the microstructure effects, which has a profound impact on the solid mechanics community. As a follow-up discussion, two simple 1D models were checked by Polyzos and Fotiadis [23] and the effectiveness of Mindlin type SG continuum model was explicitly confirmed. Then, a new truncating method for the higher-order SG terms of displacement Taylor expansions was adopted by De Domenico et al. [24]. As a result, it could be found that the continuum model works well in the long-wave range and shows the instability in certain short-wave range. It is of significance to establish an effective continuum model to predict the dispersion behavior of periodic system.

Furthermore, the continuum model of metamaterials with local resonators has also been developed. Through the introduction of additional kinematic variables, Huang et al. [8] firstly proposed the multi-displacement continuum model for 1D metamaterial with mass-in-mass structure. Then, the multi-displacement continuum model for 2D elastic metamaterials with resonators was further developed by Zhu et al. [25]. The more complex nonlocal strain gradient continuum model was proposed by Zhou et al. [26] and Zhou et al. [27]. By considering the nonlocal effects, the corresponding continuum model is unconditionally stable, but it still cannot quite accurately predict the dispersive behavior of lattice structure in the entire first Brillouin zone [21]. Although the above problem can be easily solved in the discrete model, an exact continuum model, which can show the excellent prediction ability, is still lacking.

In addition, the effects of prestress on periodic structures are also worth discussing. Bigoni et al. [28] firstly proposed the prestress as an applicable way to reversibly change the dispersive diagrams of the periodic structure. Efforts were devoted to studying the effects of prestress on band gaps structure of periodic system [29, 30]. Apart from theoretical researches and numerical analysis, some relevant experiments have also been carried out to discuss the tuning of band-gap of phononic crystals with prestress. The mechanism of the shift of band gaps in phononic crystal, with different initial stress/confining pressure, was studied experimentally [31, 32]. The above work can provide reference for tuning the band gap of periodic structure, and it is rewarding to investigate the influence of nonlocal springs on lattice system. Challamel et al. [33] studied the scale effect and higher-order boundary conditions lattices with direct and indirect elastic interactions. Challamel et al. [34] discussed the effects of long-range interactions in the longitudinal vibration of the axial lattice. The influence of long-range interactions on wave propagation and dispersion characteristics of 1D infinite acoustic metamaterials was investigated by Ghavanloo and Fazelzadeh [35]. The effects of complex nonlocal interactions on the mechanical behavior of lattice metamaterials need to be further investigated.

In this work, we try to develop an exact SG continuum model, which can successfully predict dispersion relation and band structures of PDL throughout the first Brillouin zone. The article is organized in eight sections. In Section 2, we establish the discrete model of 1D PDL, exhibit the corresponding dispersive diagrams and analyze the movement of different mass particles. In Section 3, we modify the Taylor expansion of displacement fields [36] and then propose a wavelength-dependent SG continuum model to capture bandgap characteristic of 1D PDL. In Section 4, we compare two results obtained from PDL and conventional lattice metamaterials [21]. In Sections 5 and 6, the influence of stiffness, mass, prestress parameters and SG orders is discussed, respectively. In Section 7, the effects of nonlocal interactions on PDL are studied. The conclusions are presented in Section 8.

## 2. Discrete model of PDL

An infinite extension for the diatomic lattice chain of one-dimensional prestressed acoustic metamaterials is taken into consideration, as shown in Figure 1(a), where the lattice is composed of the periodic arrangement of multiple particles and springs. From Figure 1(a), there are two kinds of atoms alternately arranged in such a diatomic lattice chain. One is composed of outer mass $M_1$ and inner mass $M_2$ and located at $\ldots 2n-2, 2n, 2n+2\ldots$. The other is composed of outer mass $m_1$ and inner mass $m_2$ and located at $\ldots 2n-1, 2n+1, 2n+3\ldots$ $a$ is the distance between each two identical atoms. The stiffness coefficients of springs between one-neighbor mass particles are $K_1$ and $K_1'$, respectively whereas those of springs between two-neighbor mass particles are $K_3$ and $K_3'$ (called "nonlocal" springs), respectively. The stiffness coefficients of internal springs, with an initial elongation $\Delta$, are, respectively, $K_2'$ and $K_2$. The original length and the length after deformation of internal springs are $\xi$ and $\ell$, respectively. For the four mass particles of the unit cell in Figure 1(a), displacement fields $u_1^{2n}$, $u_2^{2n}$, $u_1^{2n+1}$ and $u_2^{2n+1}$ are discrete counterparts of displacements of $M_1$, $M_2$, $m_1$ and $m_2$, respectively. Briefly, $u_1^{(j)}$ and $u_2^{(j)}$ represent the displacements of the outer and inner mass particles at any position $j$, respectively, where $j = \ldots 2n-2,\ 2n-1,\ 2n,\ 2n+1,\ 2n+2\ldots$ In addition, we assume that the springs here are all massless.

For different mass particles in the $n$th unit cell chosen as shown in Figure 1(a), the corresponding equations of motion,

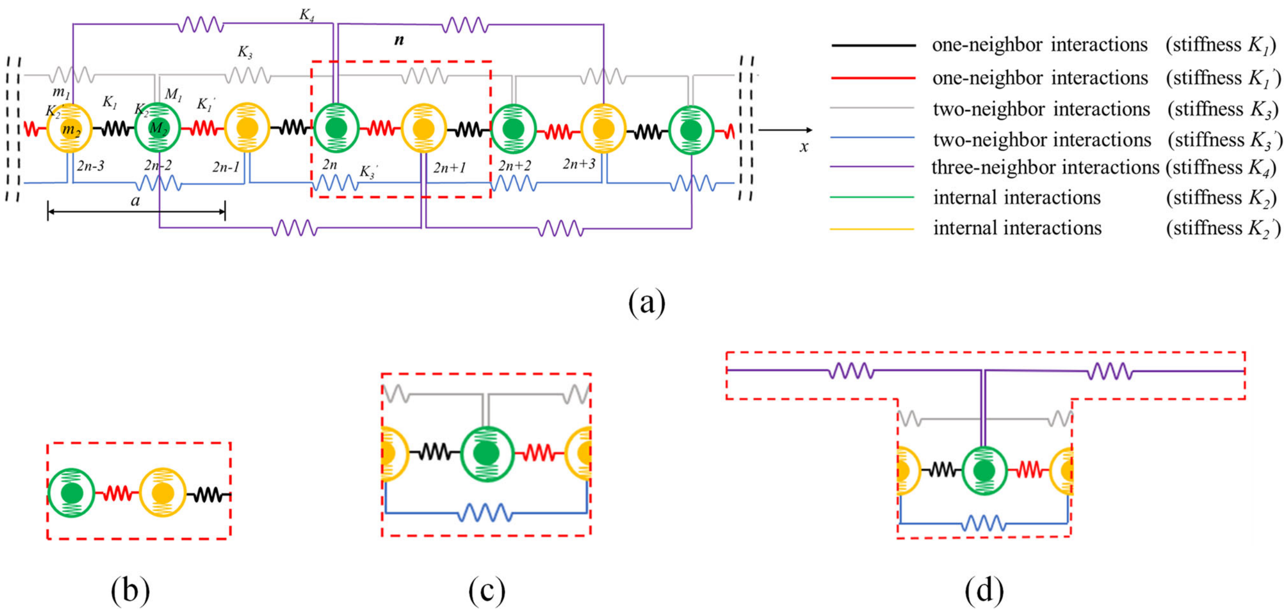


**Figure 1.** (a) 1D PDL with up to 3-neighbor interactions and unit cells for lattices with up to (b) 1-neighbor; (c) 2-neighbor and (d) 3-neighbor interactions.

hereinafter referred to as EOMs, are expressed as [21]

$$M_1\frac{d^2u_1^{(2n)}}{dt^2}=K_1'\left(u_1^{(2n+1)}-u_1^{(2n)}\right)-K_1\left(u_1^{(2n)}-u_1^{(2n-1)}\right)+K_3\left(u_1^{(2n+2)}-u_1^{(2n)}\right)-K_3\left(u_1^{(2n)}-u_1^{(2n-2)}\right)+2K_2\left[\sqrt{\ell^2+\left(u_2^{(2n)}-u_1^{(2n)}\right)^2}-\xi\right]\frac{u_2^{(2n)}-u_1^{(2n)}}{\sqrt{\ell^2+\left(u_2^{(2n)}-u_1^{(2n)}\right)^2}},\tag{1}$$

$$M_2\frac{d^2u_2^{(2n)}}{dt^2}=-2K_2\left[\sqrt{\ell^2+\left(u_2^{(2n)}-u_1^{(2n)}\right)^2}-\xi\right]\frac{u_2^{(2n)}-u_1^{(2n)}}{\sqrt{\ell^2+\left(u_2^{(2n)}-u_1^{(2n)}\right)^2}},\tag{2}$$

$$m_1\frac{d^2u_1^{(2n+1)}}{dt^2}=K_1\left(u_1^{(2n+2)}-u_1^{(2n+1)}\right)-K_1'\left(u_1^{(2n+1)}-u_1^{(2n)}\right)+K_3'\left(u_1^{(2n+3)}-u_1^{(2n+1)}\right)-K_3'\left(u_1^{(2n+1)}-u_1^{(2n-1)}\right)+2K_2'\left[\sqrt{\ell^2+\left(u_2^{(2n+1)}-u_1^{(2n+1)}\right)^2}-\xi\right]\frac{u_2^{(2n+1)}-u_1^{(2n+1)}}{\sqrt{\ell^2+\left(u_2^{(2n+1)}-u_1^{(2n+1)}\right)^2}},\tag{3}$$

$$m_2\frac{d^2u_2^{(2n+1)}}{dt^2}=-2K_2'\left[\sqrt{\ell^2+\left(u_2^{(2n+1)}-u_1^{(2n+1)}\right)^2}-\xi\right]\frac{u_2^{(2n+1)}-u_1^{(2n+1)}}{\sqrt{\ell^2+\left(u_2^{(2n+1)}-u_1^{(2n+1)}\right)^2}}.\tag{4}$$

To avoid the nonlinear case, we assume that the relative displacement is much smaller than the initial deformation of the internal spring, that is, $u_2^{(j)}-u_1^{(j)}\ll\Delta$. Based on this assumption, Eqs. (1)–(4) can be rewritten as

$$M_1\frac{d^2u_1^{(2n)}}{dt^2}=K_1'\left(u_1^{(2n+1)}-u_1^{(2n)}\right)-K_1\left(u_1^{(2n)}-u_1^{(2n-1)}\right)+2K_2\frac{\Delta}{\ell}\left(u_2^{(2n)}-u_1^{(2n)}\right)+K_3\left(u_1^{(2n+2)}-u_1^{(2n)}\right)-K_3\left(u_1^{(2n)}-u_1^{(2n-2)}\right),\tag{5}$$

$$M_2\frac{d^2u_2^{(2n)}}{dt^2}=-2K_2\frac{\Delta}{\ell}\left(u_2^{(2n)}-u_1^{(2n)}\right),\tag{6}$$

$$m_1\frac{d^2u_1^{(2n+1)}}{dt^2}=K_1\left(u_1^{(2n+2)}-u_1^{(2n+1)}\right)-K_1'\left(u_1^{(2n+1)}-u_1^{(2n)}\right)+2K_2'\frac{\Delta}{\ell}\left(u_2^{(2n+1)}-u_1^{(2n+1)}\right)+K_3'\left(u_1^{(2n+3)}-u_1^{(2n+1)}\right)-K_3'\left(u_1^{(2n+1)}-u_1^{(2n-1)}\right),\tag{7}$$

$$m_2\frac{d^2u_2^{(2n+1)}}{dt^2}=-2K_2'\frac{\Delta}{\ell}\left(u_2^{(2n+1)}-u_1^{(2n+1)}\right).\tag{8}$$

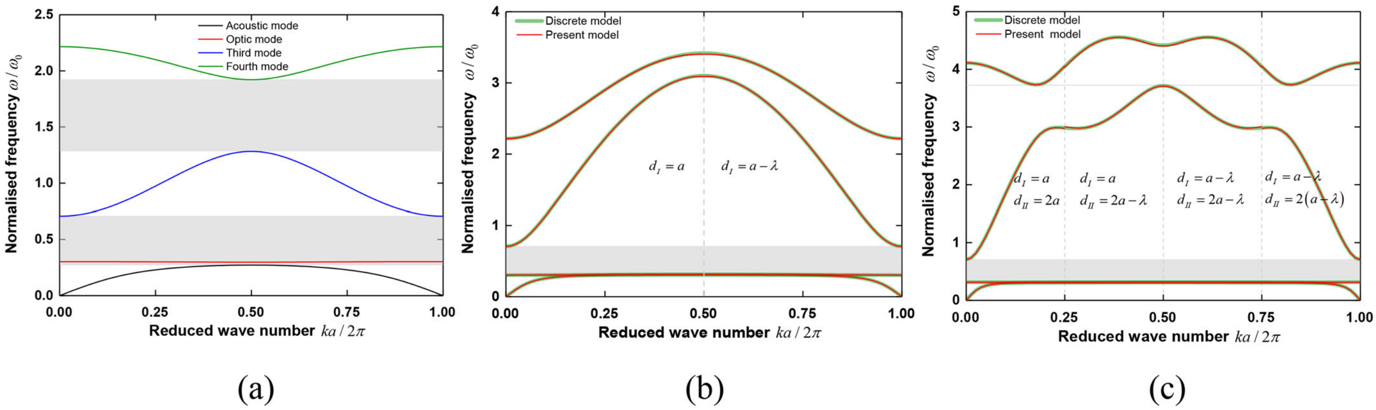


**Figure 2.** Dispersion curves of PDL with up to (a) one-; (b) two- and (c) three-neighbor interactions, obtained by the discrete and/or present models. Dimensionless parameters are defined as follows: $\alpha = 4,\ \beta = 2,\ \alpha_0 = 2,\ \beta_0 = 0.5,\ \gamma = 2,\ \gamma_0 = 1,\ \theta = 2$ and $\frac{\Delta}{\ell} = 0.1$.

The solutions to the lattice wave are

$$\begin{aligned} u_1^{(2n)} &= A_1 e^{i(kx-\omega t)}, u_1^{(2n+1)} = B_1 e^{i(kx-\omega t)}, \\ u_1^{(2n-1)} &= B_1 e^{i[k(x-a)-\omega t]}, u_1^{(2n+3)} = B_1 e^{i[k(x+a)-\omega t]}, \\ u_2^{(2n)} &= A_2 e^{i(kx-\omega t)}, u_2^{(2n+1)} = B_2 e^{i(kx-\omega t)}, \\ u_1^{(2n+2)} &= A_1 e^{i[k(x+a)-\omega t]}, u_1^{(2n-2)} = A_1 e^{i[k(x-a)-\omega t]}, \end{aligned} \tag{9}$$

where $A_1,\ A_2,\ B_1$ and $B_2$ are the amplitudes of lattice wave, $k$ is the wave number and $\omega$ is the angular frequency.

Substituting Eq. (9) into Eqs. (5)–(8) yields

$$\begin{aligned} &\left[M_1\omega^2 - K_1' - K_1 - 2\frac{\Delta}{\ell}K_2 - 2K_3 + 2K_3\cos(ka)\right]A_1 \\ &+ 2\frac{\Delta}{\ell}K_2A_2 + \left(K_1' + K_1e^{-ika}\right)B_1 = 0, \end{aligned} \tag{10}$$

$$2\frac{\Delta}{\ell}K_2A_1 + \left(M_2\omega^2 - 2\frac{\Delta}{\ell}K_2\right)A_2 = 0, \tag{11}$$

$$\begin{aligned} &\left(K_1e^{ika} + K_1'\right)A_1 + \left[m_1\omega^2 - K_1 - K_1' - 2\frac{\Delta}{\ell}K_2'\right. \\ &\left. -2K_3' + 2K_3'\cos(ka)\right]B_1 + 2\frac{\Delta}{\ell}K_2'B_2 = 0, \end{aligned} \tag{12}$$

$$2\frac{\Delta}{\ell}K_2'B_1 + \left(m_2\omega^2 - 2\frac{\Delta}{\ell}K_2'\right)B_2 = 0. \tag{13}$$

By requesting that $A_1,\ A_2,\ B_1$ and $B_2$ have non-zero solutions, we get

$$\begin{vmatrix} \left(\frac{\omega}{\omega_0}\right)^2 - 2\frac{\Delta}{\ell}\beta - \beta_0 - 1 - 2\gamma + 2\gamma\cos(ka) & 2\frac{\Delta}{\ell}\beta & \beta_0 + e^{-ika} & 0 \\ 2\frac{\Delta}{\ell}\beta & \alpha\left(\frac{\omega}{\omega_0}\right)^2 - 2\frac{\Delta}{\ell}\beta & 0 & 0 \\ e^{ika} + \beta_0 & 0 & \frac{1}{\alpha_0}\left(\frac{\omega}{\omega_0}\right)^2 - 2\frac{\Delta}{\ell}\beta\beta_0 - \beta_0 - 1 - 2\gamma_0 + 2\gamma_0\cos(ka) & 2\frac{\Delta}{\ell}\beta\beta_0 \\ 0 & 0 & 2\frac{\Delta}{\ell}\beta\beta_0 & \frac{\alpha}{\alpha_0}\left(\frac{\omega}{\omega_0}\right)^2 - 2\frac{\Delta}{\ell}\beta\beta_0 \end{vmatrix} = 0, \tag{14}$$

where we make the following parameter settings: $\alpha = \frac{M_2}{M_1} = \frac{m_2}{m_1}, \beta = \frac{K_2}{K_1} = \frac{K'_2}{K'_1}, \alpha_0 = \frac{M_1}{m_1}, \beta_0 = \frac{K'_1}{K_1},\ \gamma = \frac{K_3}{K_1},\ \gamma_0 = \frac{K_3'}{K_1}$ and $\omega_0^2 = \frac{K_1}{M_1}$. The dispersion relation of PDL is given by Eq. (14).

If $K_3 = K_3' = 0$ in Eq. (14), the PDL with local and two-neighbor interactions reduces to be that only with one-neighbor interactions and then corresponding dispersion relation is

Figure 2(a) depicts the dispersion curves of PDL. Similar to the wave in conventional diatomic lattice [21] without prestress, the wave still has four branches, which are the acoustic, optical, third and fourth branches, respectively. The adjustability of three band gaps appearing in the dispersive diagram is enhanced when the corresponding prestress parameter is introduced, which contributes to the metamaterial design.

Moreover, the movement of particles in a periodic cell deserves to be discussed. Setting $K_3 = K_3' = 0$ in Eqs. (10)–(13), we obtain

$$\left[\left(\frac{\omega}{\omega_0}\right)^2 - 2\frac{\Delta}{\ell}\beta - \beta_0 - 1\right]A_1 + 2\frac{\Delta}{\ell}\beta A_2 + \left(\beta_0 + e^{-ika}\right)B_1 = 0, \tag{16}$$

$$2\frac{\Delta}{\ell}\beta A_1 + \left[\alpha\left(\frac{\omega}{\omega_0}\right)^2 - 2\frac{\Delta}{\ell}\beta\right]A_2 = 0, \tag{17}$$

$$\begin{vmatrix} \left(\frac{\omega}{\omega_0}\right)^2-2\frac{\Delta}{\ell}\beta-\beta_0-1 & 2\frac{\Delta}{\ell}\beta & e^{-ika}+\beta_0 & 0 \\ 2\frac{\Delta}{\ell}\beta & \alpha\left(\frac{\omega}{\omega_0}\right)^2-2\frac{\Delta}{\ell}\beta & 0 & 0 \\ e^{ika}+\beta_0 & 0 & \frac{1}{\alpha_0}\left(\frac{\omega}{\omega_0}\right)^2-2\frac{\Delta}{\ell}\beta\beta_0-\beta_0-1 & 2\frac{\Delta}{\ell}\beta\beta_0 \\ 0 & 0 & 2\frac{\Delta}{\ell}\beta\beta_0 & \frac{\alpha}{\alpha_0}\left(\frac{\omega}{\omega_0}\right)^2-2\frac{\Delta}{\ell}\beta\beta_0 \end{vmatrix}=0. \tag{15}$$

$$\left(e^{ika}+\beta_0\right)A_1+\left[\frac{1}{\alpha_0}\left(\frac{\omega}{\omega_0}\right)^2-2\frac{\Delta}{\ell}\beta\beta_0-\beta_0-1\right]B_1 + 2\frac{\Delta}{\ell}\beta\beta_0B_2=0, \tag{18}$$

$$2\frac{\Delta}{\ell}\beta\beta_0B_1+\left[\frac{\alpha}{\alpha_0}\left(\frac{\omega}{\omega_0}\right)^2-2\frac{\Delta}{\ell}\beta\beta_0\right]B_2=0. \tag{19}$$

According to Eqs. (16)–(19), the corresponding amplitude ratios can be given as

$$\frac{B_1}{A_1}=-\left(\beta_0+e^{-ika}\right)^{-1}\left[\left(\frac{\omega}{\omega_0}\right)^2-2\frac{\Delta}{\ell}\beta-\beta_0-1+\frac{\left(2\frac{\Delta}{\ell}\beta\right)^2}{2\frac{\Delta}{\ell}\beta-\alpha\left(\frac{\omega}{\omega_0}\right)^2}\right], \tag{20}$$

$$\frac{A_2}{A_1}=\frac{2\frac{\Delta}{\ell}\beta}{2\frac{\Delta}{\ell}\beta-\alpha\left(\frac{\omega}{\omega_0}\right)^2}, \tag{21}$$

$$\frac{B_2}{A_1}=-\frac{\left(e^{ika}+\beta_0\right)}{2\frac{\Delta}{\ell}\beta\beta_0}+\frac{1}{2\frac{\Delta}{\ell}\beta\beta_0\left(\beta_0+e^{-ika}\right)}\left[\frac{1}{\alpha_0}\left(\frac{\omega}{\omega_0}\right)^2-2\frac{\Delta}{\ell}\beta\beta_0-\beta_0-1\right]\left[\left(\frac{\omega}{\omega_0}\right)^2-2\frac{\Delta}{\ell}\beta-\beta_0-1+\frac{\left(2\frac{\Delta}{\ell}\beta\right)^2}{2\frac{\Delta}{\ell}\beta-\alpha\left(\frac{\omega}{\omega_0}\right)^2}\right]. \tag{22}$$

Equations (20)–(22) are the amplitude ratios of particle vibrations, respectively.

We adopt the aforementioned parameters to reveal relative motions of particles in the specific case. The relation curves that amplitude ratios vary with reduced wave number $\frac{ka}{2\pi}$ are obtained in Figure 3. Figure 3(a–d) shows the results for the acoustic, optical, third and fourth branches, respectively. As shown in Figure 3(a), when $\frac{ka}{2\pi}\to 0$, amplitude ratios $\frac{B_1}{A_1}$, $\frac{B_2}{A_1}$ and $\frac{A_2}{A_1}$ are all close to 1. This suggests that for the long acoustic wave, several particles in the same unit cell actually move together like a rigid unit. From Figure 3(a,b), we find that $\frac{A_2}{A_1}>0$ is always true in the whole first Brillouin zone, which means that particles $M_2$ and $M_1$ always move in the same direction. Furthermore, in Figure 3(a–d), there are also negative amplitude ratios, indicating that the corresponding two particles vibrate in the opposite direction. In Figure 3(d), it is worth noting that amplitude ratios $\frac{B_2}{A_1}$ and $\frac{A_2}{A_1}$ are very close to 0, suggesting that mass particles $M_2$ and $m_2$ are approximately at rest. From Figure 3(a–d), in most situations, the movement of each mass particle in the same unit cell is different. The lattice wave motion obviously violates the Cauchy–Born (C–B) continuity hypothesis. For the PDL discussed in this study, the displacement fields of all mass particles $M_1$, follow the C–B continuity hypothesis, and so do those of mass particles $M_2$, $m_1$ and $m_2$. Therefore, there are four kinds of continuous displacement fields (called multi-displacement method) at the same time. In other words, the above results indicate that continuity of displacement field in the periodic unit cell is destroyed and the incursion of the multi-displacement method is imperative.

## 3. Exact SG continuum model with a wavelength-dependent Taylor expansion

With the Taylor expansion of displacements modified, the wavelength-dependent SG continuum model of PDL is proposed here. The model only with one-neighbor interactions is studied and that with more complex interactions is discussed in Section 7. The selected periodic unit cell framed by a red dashed line is presented in Figure 1(b), which consists of four complete mass particles, two one-neighbor springs and four internal springs with initial deformation.

Four continuous displacement fields corresponding to the mass particles of the chosen unit cell in Figure 1(b) are

$$u_1^{(2n)}=u_1(x,t),\ u_2^{(2n)}=\tilde{u}_1(x,t),\ u_1^{(2n+1)}=u_2(x,t),\ u_2^{(2n+1)}=\tilde{u}_2(x,t), \tag{23}$$

The displacements of adjacent mass particles can be written as

$$u_1^{(2n\pm2)}=u_1(x\pm a,t),\ u_1^{(2n-1)}=u_2(x-a,t) \tag{24}$$

The Taylor expansion of displacements of one- and two-neighbor mass particles is modified to make results obtained from SG continua more accurate. Thus, Eq. (24) can be rewritten as

$$u_1(x\pm a,t)=u_1(x\pm d_I,t)=u_1+\sum_{p=1}^{\infty}(\pm1)^p\frac{d_I^p}{p!}\frac{\partial^p u_1}{\partial x^p},$$
$$u_2(x\pm a,t)=u_2(x\pm d_I,t)=u_2+\sum_{p=1}^{\infty}(\pm1)^p\frac{d_I^p}{p!}\frac{\partial^p u_2}{\partial x^p}. \tag{25}$$

where the value of $d_I$ depends on the wavelength $\lambda$ and is not

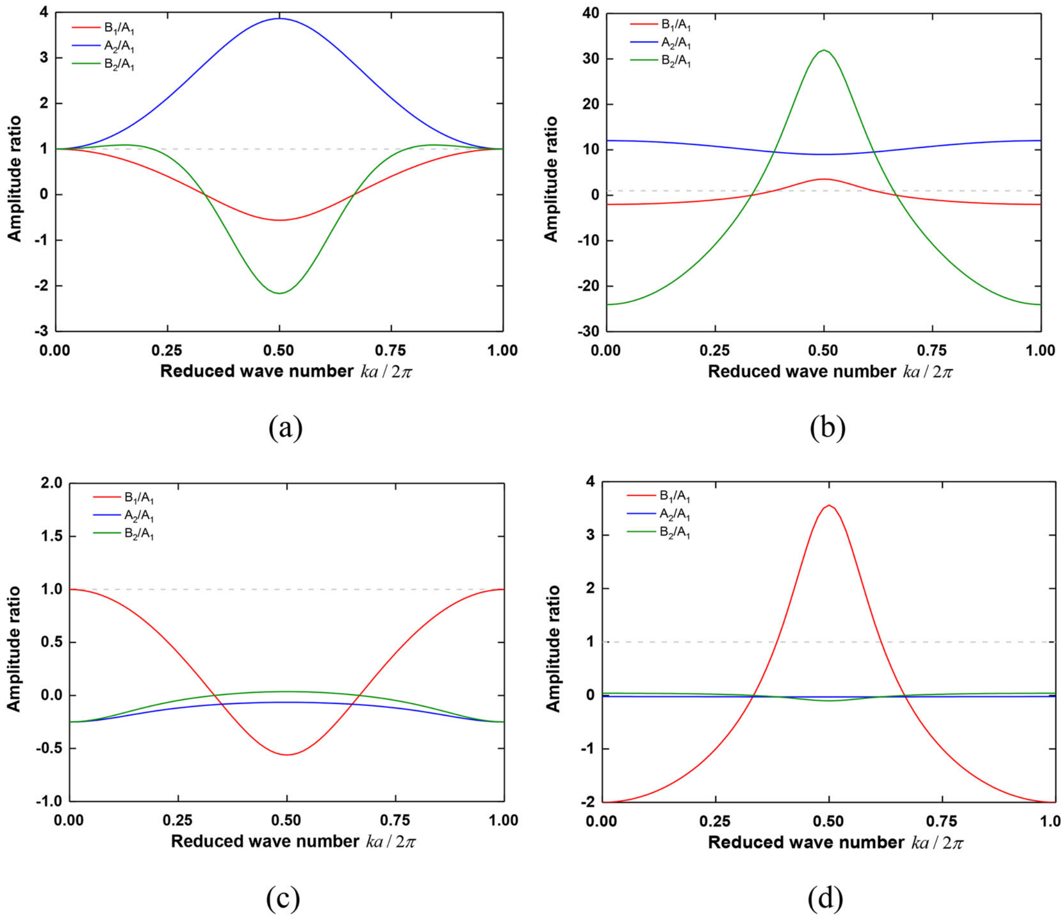


**Figure 3.** Diagrams of vibration amplitude ratios corresponding to the (a) acoustic, (b) optic, (c) third and (d) fourth branches in Figure 2(a) when $\alpha=4,\ \beta=2,\ \alpha_0=2,\ \beta_0=0.5$ and $\frac{\Delta}{\ell}=0.1$.

directly set as the lattice spacing $a$. For 1D problems, the partial derivative $u_1'=\frac{\partial u_1}{\partial x}$ refers to the normal strain and the $n$th-order partial derivative of strain, such as $u_1''$, $u_1'''$ and $u_1^{(4)}$, is called the strain gradient. When the wavelength $\lambda$ is much larger than the microstructure spacing $a$, we adopt $d_I=a$, as most continuum theories have been done under the so-called long-wave approximation. However, when the wavelength $\lambda$ is close to $a$, the so-called long-wave approximation does not work, which is also the issue we focus on. According to the periodicity of wave motion, the displacements at the position $x\pm\lambda$ are equal to those at $x$, i.e.,

$$u_1(x\pm\lambda,t)=u_1(x,t),u_2(x\pm\lambda,t)=u_2(x,t). \tag{26}$$

If we want to get the Taylor expansion of the displacement located at $x\pm a$, to ensure the accuracy, we require to decide which of $x\pm\lambda$ and $x$ is closest to $x\pm a$, select the nearest position point and then set the distance between $x\pm a$ and that position point as $d_I$. As shown in Figure 4, displacements located at $x+l\lambda\ (l=0,\pm1,\pm2,\pm3\cdots)$ are equal to those located at $x$, and the Taylor expansion should be carried out according to the nearest location among all $x+l\lambda$.

Based on the above discussion of motion periodicity, we can obtain

$$d_I=\begin{cases} a-\lambda & \text{when } \lambda\in[a,2a] \\ a & \text{when } \lambda\in(2a,\infty) \end{cases} \tag{27}$$

Then, the potential energy density and kinetic energy density for the chosen unit cell are, respectively

$$W=\frac{1}{2Aa}\left[K_1\left(u_1^{(2n+2)}-u_1^{(2n+1)}\right)^2+K_1'\left(u_1^{(2n+1)}-u_1^{(2n)}\right)^2 +2\frac{\Delta}{\ell}K_2\left(u_2^{(2n)}-u_1^{(2n)}\right)^2+2\frac{\Delta}{\ell}K_2'\left(u_2^{(2n+1)}-u_1^{(2n+1)}\right)^2\right] \tag{28}$$

$$T=\frac{1}{2Aa}\left[M_1\left(\dot{u}_1^{(2n)}\right)^2+M_2\left(\dot{u}_2^{(2n)}\right)^2+m_1\left(\dot{u}_1^{(2n+1)}\right)^2 +m_2\left(\dot{u}_2^{(2n+1)}\right)^2\right], \tag{29}$$

where $Aa$ refers to the volume of the unit cell containing four whole mass particles, and is not dependent on the selection of springs. The same is true in the following discussion.

Substituting Eqs. (23)–(25) into Eqs. (28) and (29) and truncating the acquired equations after the $d_I^8$, we get

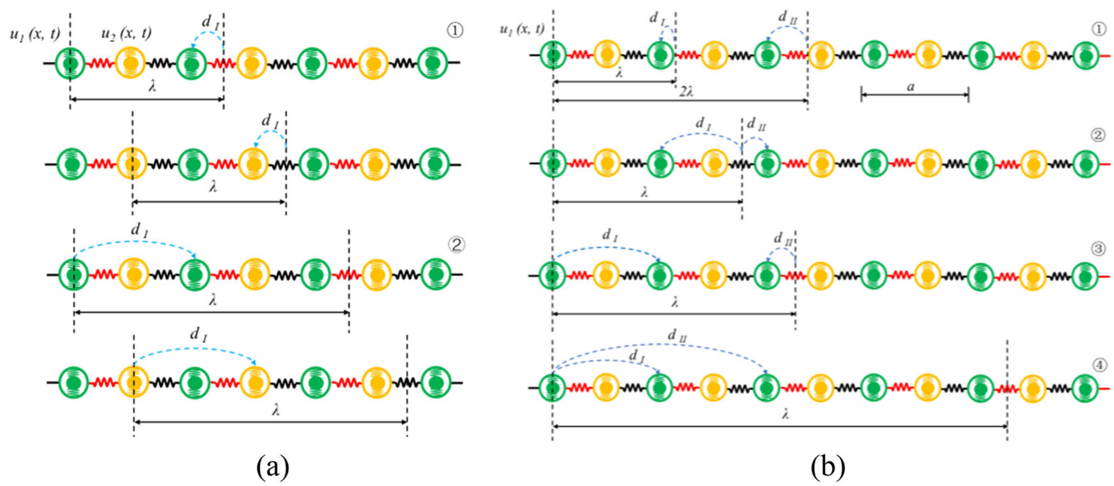

Figure 4. Wavelength-dependent values of $d_I$ and $d_{II}$ for PDL with interactions of up to (a) one- and two-neighbor: ① $a \le \lambda \le 2a$, ② $\lambda > 2a$; and (b) three-neighbor: ① $a \le \lambda \le 4a/3$, ② $4a/3 < \lambda \le 2a$, ③ $2a < \lambda \le 4a$ and ④ $\lambda > 4a$.

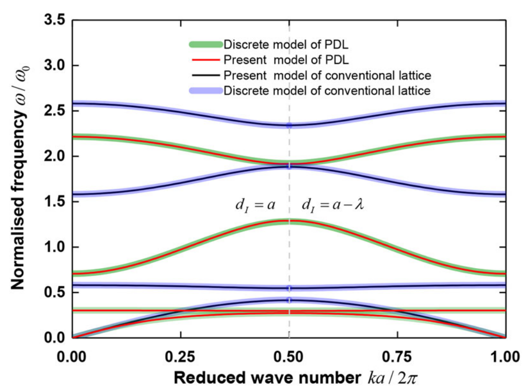


Figure 5. Comparison of the present and discrete models of PDL and conventional lattice when parameters are set as $\alpha = 4$, $\beta = 2$, $\alpha_0 = 2$, $\beta_0 = 0.5$ and $\frac{\Delta}{\ell} = 0.1$.

$$W = \frac{1}{2Aa}\left[K_1\left(u_1 + \sum_{p=1}^{8}\frac{d_I^p}{p!}\frac{\partial^p u_1}{\partial x^p} - u_2\right)^2 + K_1'(u_2 - u_1)^2 + 2\frac{\Delta}{\ell}K_2(\tilde{u}_1 - u_1)^2 + 2\frac{\Delta}{\ell}K_2'(\tilde{u}_2 - u_2)^2\right] \tag{30}$$

$$T = \frac{1}{2Aa}\left[M_1\dot{u}_1^2 + M_2\left(\dot{\tilde{u}}_1\right)^2 + m_1\dot{u}_2^2 + m_2\left(\dot{\tilde{u}}_2\right)^2\right]. \tag{31}$$

Adopting the Hamilton variation principle, i.e.,

$$\delta\int_{t_1}^{t_2}\int_V (T - W)dVdt = 0, \tag{32}$$

we obtain the EOMs:

$$M_1\ddot{u}_1 + \left(K_1 + K_1' + 2\frac{\Delta}{\ell}K_2\right)u_1 - 2\frac{\Delta}{\ell}K_2\tilde{u}_1 - (K_1 + K_1')u_2 + K_1\sum_{p=1}^{8}(-1)^{p+1}\frac{d_I^p}{p!}\frac{\partial^p u_2}{\partial x^p} = 0, \tag{33}$$

$$M_2\ddot{\tilde{u}}_1 + 2\frac{\Delta}{\ell}K_2(\tilde{u}_1 - u_1) = 0, \tag{34}$$

$$m_1\ddot{u}_2 - (K_1 + K_1')u_1 + \left(K_1 + K_1' + 2\frac{\Delta}{\ell}K_2'\right)u_2 - 2\frac{\Delta}{\ell}K_2'\tilde{u}_2 - K_1\sum_{p=1}^{8}\frac{d_I^p}{p!}\frac{\partial^p u_1}{\partial x^p} = 0, \tag{35}$$

$$m_2\ddot{\tilde{u}}_2 + 2\frac{\Delta}{\ell}K_2'(\tilde{u}_2 - u_2) = 0. \tag{36}$$

Equations (33)–(36) provide the evolutions of the continuous displacements including $u_1(x,t)$, $\tilde{u}_1(x,t)$, $u_2(x,t)$ and $\tilde{u}_2(x,t)$ in terms of $x$ and $t$. Therefore, it can be taken as a continuum model for the studied PDL, just as done by De Domenico et al. [24] and Polyzos and Fotiadis [23].

The continuous displacement solutions are

$$\begin{aligned} u_1 &= C_1e^{i(kx-\omega t)}, & \tilde{u}_1 &= C_2e^{i(kx-\omega t)}, \\ u_2 &= D_1e^{i(kx-\omega t)}, & \tilde{u}_2 &= D_2e^{i(kx-\omega t)}. \end{aligned} \tag{37}$$

Substituting Eq. (37) into Eqs. (33)–(36) yields

$$M_1\omega^2C_1 - \left(K_1 + K_1' + 2\frac{\Delta}{\ell}K_2\right)C_1 + 2\frac{\Delta}{\ell}K_2C_2 + (K_1 + K_1')D_1 - K_1\sum_{p=1}^{8}(-1)^{p+1}\frac{(ikd_I)^p}{p!}D_1 = 0, \tag{38}$$

$$2\frac{\Delta}{\ell}K_2C_1 + \left(M_2\omega^2 - 2\frac{\Delta}{\ell}K_2\right)C_2 = 0, \tag{39}$$

$$m_1\omega^2D_1 + (K_1 + K_1')C_1 - \left(K_1 + K_1' + 2\frac{\Delta}{\ell}K_2'\right)D_1 + 2\frac{\Delta}{\ell}K_2'D_2 + K_1\sum_{p=1}^{8}\frac{(ikd_I)^p}{p!}C_1 = 0, \tag{40}$$

$$2\frac{\Delta}{\ell}K_2'D_1 + \left(m_2\omega^2 - 2\frac{\Delta}{\ell}K_2'\right)D_2 = 0. \tag{41}$$

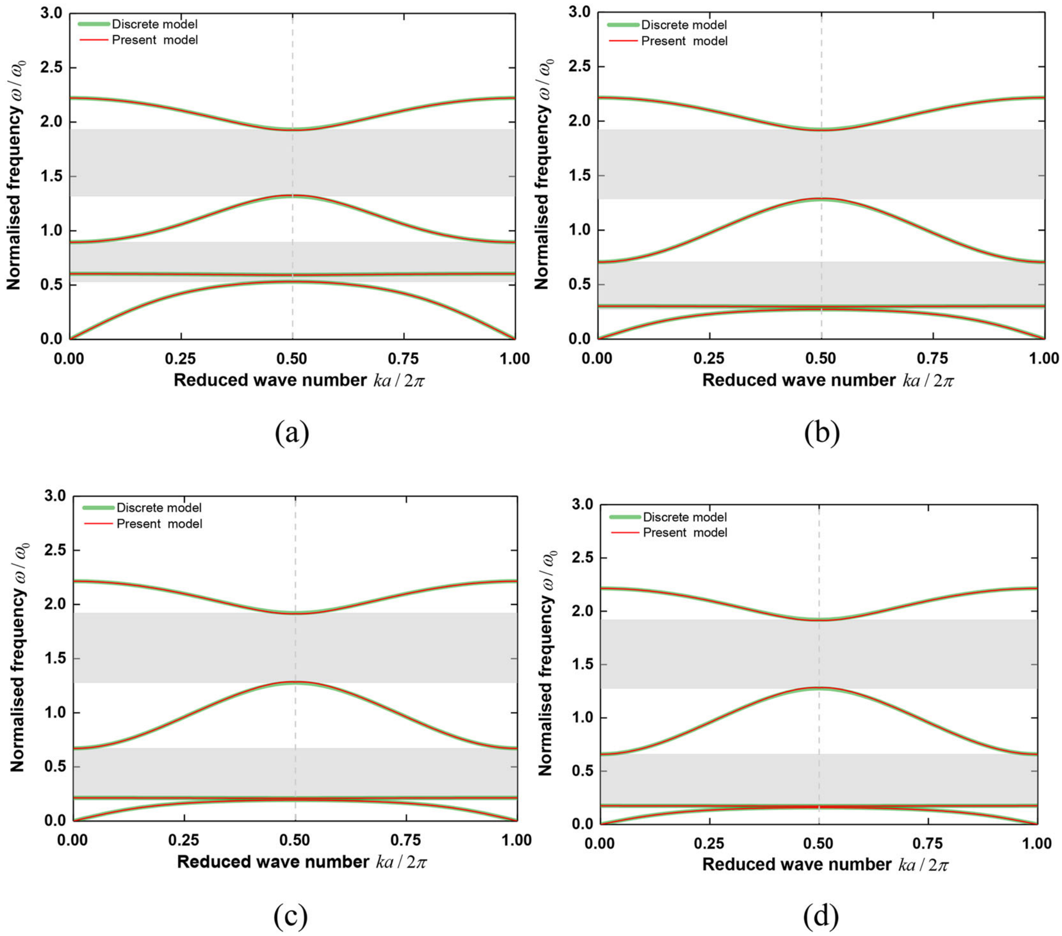


**Figure 6.** Dispersion curves of the discrete and present SG models when $\frac{M_2}{M_1}=\frac{m_2}{m_1}$ is set as (a) 1; (b) 4; (c) 8 and (d) 12. For all cases, $\frac{K_2}{K_1}=\frac{K_2'}{K_1'}=2$, $\frac{\Delta}{\ell}=0.1$, $\frac{M_1}{m_1}=2$ and $\frac{K_1'}{K_1}=0.5$.

Equations (38)–(41) are the dispersive equations of the exact SG continuum model.

Introducing the dimensionless parameters mentioned in Section 2 and setting the determinant of the coefficient matrix of Eqs. (38)–(41) to be zero, which ensures that a nontrivial solution exists, the dispersive equation can be written as

$$\begin{vmatrix} \left(\frac{\omega}{\omega_0}\right)^2-2\frac{\Delta}{\ell}\beta-\beta_0-1 & 2\frac{\Delta}{\ell}\beta & \beta_0+1-\eta_1 & 0 \\ 2\frac{\Delta}{\ell}\beta & \alpha\left(\frac{\omega}{\omega_0}\right)^2-2\frac{\Delta}{\ell}\beta & 0 & 0 \\ 1+\beta_0+\eta_2 & 0 & \frac{1}{\alpha_0}\left(\frac{\omega}{\omega_0}\right)^2-2\frac{\Delta}{\ell}\beta\beta_0-\beta_0-1 & 2\frac{\Delta}{\ell}\beta\beta_0 \\ 0 & 0 & 2\frac{\Delta}{\ell}\beta\beta_0 & \frac{\alpha}{\alpha_0}\left(\frac{\omega}{\omega_0}\right)^2-2\frac{\Delta}{\ell}\beta\beta_0 \end{vmatrix}=0. \tag{42}$$

where $\eta_1=\sum_{p=1}^{8}(-1)^{p+1}\frac{(ikd_l)^p}{p!}$ and $\eta_2=\sum_{p=1}^{8}\frac{(ikd_l)^p}{p!}$.

Similarly, the displacement amplitude ratios corresponding to the proposed continuum model are also derived, i.e.,

$$\frac{D_1}{C_1}=-\left(\beta_0+1-\eta_1^+\right)^{-1}\left[\left(\frac{\omega}{\omega_0}\right)^2-2\frac{\Delta}{\ell}\beta-\beta_0-1+\frac{\left(2\frac{\Delta}{\ell}\beta\right)^2}{2\frac{\Delta}{\ell}\beta-\alpha\left(\frac{\omega}{\omega_0}\right)^2}\right], \tag{43}$$

$$\frac{C_2}{C_1}=\frac{2\frac{\Delta}{\ell}\beta}{2\frac{\Delta}{\ell}\beta-\alpha\left(\frac{\omega}{\omega_0}\right)^2}, \tag{44}$$

$$\frac{D_2}{C_1}=-\frac{\beta_0+1+\eta_2^+}{2\frac{\Delta}{\ell}\beta\beta_0}+\frac{1}{2\frac{\Delta}{\ell}\beta\beta_0\left(\beta_0+1-\eta_1^+\right)}\left[\frac{1}{\alpha_0}\left(\frac{\omega}{\omega_0}\right)^2-2\frac{\Delta}{\ell}\beta\beta_0-\beta_0-1\right]\left[\left(\frac{\omega}{\omega_0}\right)^2-2\frac{\Delta}{\ell}\beta-\beta_0-1+\frac{\left(2\frac{\Delta}{\ell}\beta\right)^2}{2\frac{\Delta}{\ell}\beta-\alpha\left(\frac{\omega}{\omega_0}\right)^2}\right], \tag{45}$$

where $\eta_1^+=\sum_{p=1}^{10}(-1)^{p+1}\frac{(ikd_l)^p}{p!}$ and $\eta_2^+=\sum_{p=1}^{10}\frac{(ikd_l)^p}{p!}$. It can be observed that Eqs. (43)–(45) are the same as their discrete counterparts, i.e., Eqs. (20)–(22).

## 4. Comparison and validation

The proposed SG continuum is discussed and applied to explore the effects of initial deformation on PDL. In this section, results obtained from discrete and continuum models of the conventional diatomic lattice [21] with mass-in-mass structure and PDL are compared. The corresponding dispersion curves are exhibited in Figure 5.

- Based on the periodicity of the displacements, we introduce the modified Taylor expansion in which the dependency of $d_I$ on wavelength $\lambda$ is emphasized. When the wavelength $\lambda$ is greater than $2a$, that is, the reduced wave number $\frac{ka}{2\pi} \in [0, 0.5]$, the corresponding value of $d_I$ is equal to particle spacing $a$. Nevertheless, when the reduced wave number $\frac{ka}{2\pi} \in [0.5, 1]$, $d_I$ is equal to $a-\lambda$ instead of $a$, as a result, the limitations of the long-wave approximation can be eliminated. As shown in Figure 5, results of the present models are in good agreement with those of the discrete models in the entire first Brillouin zone, suggesting that the present model can effectively predict the dispersion relation of the corresponding discrete model. Note that we only adopt the eighth-order truncation of $d_I$ and we will explain the effects of orders in the next discussion.
- The existence of prestress obviously affects bandgap characteristics of the diatomic lattice. Under the action of prestress, inner springs have a certain elongation $\Delta$. Figure 5 shows the variation of dispersion curves when $\frac{\Delta}{\ell} = 0.1$. Due to the introduction of prestress, four branches of the dispersive curves for the corresponding models shift to low-frequency region. Relative to the original lattice, the lower frequency band gap is more likely to occur. The frequency range of the first band gap (from bottom to top) is extremely shrunk and close to 0 whereas that of the third one becomes wider. Also, the width of the second band gap decreases. It can be found that the introduction of prestress parameter contributes to provide a reliable approach to adjusting band gaps distribution.

## 5. Influences of prestress parameter ($\frac{\Delta}{\ell}$), mass ratio ($\frac{M_2}{M_1} = \frac{m_2}{m_1}$) and stiffness ratio ($\frac{K_2}{K_1} = \frac{K_2'}{K_1'}$): 1D diatomic chain with local interactions as an example

The band gap characteristics of the original 1D diatomic lattice are only affected by mass parameter $\alpha = \frac{M_2}{M_1} = \frac{m_2}{m_1}$ and stiffness parameter $\beta = \frac{K_2}{K_1} = \frac{K_2'}{K_1'}$. Here, we define an additional parameter, $\frac{\Delta}{\ell}$, to describe the influence of the internal springs with prestress on the band gap structure. The detailed changes of the dispersion curves and band gaps with the above three parameters are displayed in Figures 6–8, respectively. Moreover, the changes of the width and lower bound of every band gap with two of three parameters are presented in Figures 9 and 10. In this section, the present model with only eighth-order truncation is adopted. In the next section, efforts will be devoted to mainly illustrating the effects of orders of SG continua.

Figure 6 depicts the influence of mass ratio on the band gap behavior of PDL. When the other parameters are constant and the mass ratio increases, the acoustic, optical and the third branches approach to the position of the lower frequency gradually whereas the fourth branch is almost unchanged. According to Figure 6(a–d), the first band gap (from bottom to top) becomes narrower and appears in the lower frequency range when the value of mass ratio $\alpha$ changes from 1 to 12. Moreover, the frequency range of the second band gap increases and that of the third one varies slightly.

Figure 7 describes the effects of stiffness ratio on the band gap behavior of PDL. As the value of stiffness ratio $\beta$ increases from 1 to 7, all four branches and the corresponding band gaps go up to the high-frequency region. Besides, the first and second band gaps are broadened evidently. In summary, fixing the prestress parameter $\frac{\Delta}{\ell}$ and changing mass and stiffness ratios are beneficial to regulating the band gap structure of PDL.

Figure 8 emphasizes the effects of initial elongation on the band gap structure. With the increase in the value of parameter $\frac{\Delta}{\ell}$, the first and second band gaps become wider whereas the third one becomes narrower. As $\frac{\Delta}{\ell}$ increases, all four branches rise to the higher frequency zone. From the above analysis, the prestress parameter plays a significant role in band gap behavior.

The starting frequency and width of every band gap deserve to be considered when designing metamaterials. The lower bound and width of every band gap are defined. Taking the first band gap between the acoustic and optical branches as an example, we briefly explain the relevant definitions. The lower bound is the maximum of the normalized frequency $\left(\frac{\omega}{\omega_0}\right)_{ac}^{\max}$ corresponding to the acoustic branch whereas the upper bound is the minimum of the normalized frequency $\left(\frac{\omega}{\omega_0}\right)_{op}^{\min}$ corresponding to the optic branch. The difference between the two bound values is the first band gap width when the band gap does exist. The same is true for other definitions. The effects of mass, stiffness and prestress parameters on widths and lower bounds of band gaps are investigated and the results are presented in Figures 9 and 10.

- Figure 9(a,c,e) shows the changes of the lower bound of each band gap with mass and prestress parameters. For three band gaps, with the increase in the parameter $\frac{\Delta}{\ell}$, the lower bounds increase whereas with the increase in the parameter $\alpha$, those decrease, meaning that for larger $\frac{\Delta}{\ell}$ and smaller $\alpha$, the larger lower bound value can be achieved. According to these analyses, we can get the desired lower bound by choosing the proper mass ratio $\alpha$ and prestress parameter $\frac{\Delta}{\ell}$.
- Similarly, Figure 9(b,d,f) describes the effects of mass and prestress parameters on the three band gap widths. For a fixed $\alpha$, the widths of the first and second band gap increase with the increase in $\frac{\Delta}{\ell}$ and that of the third

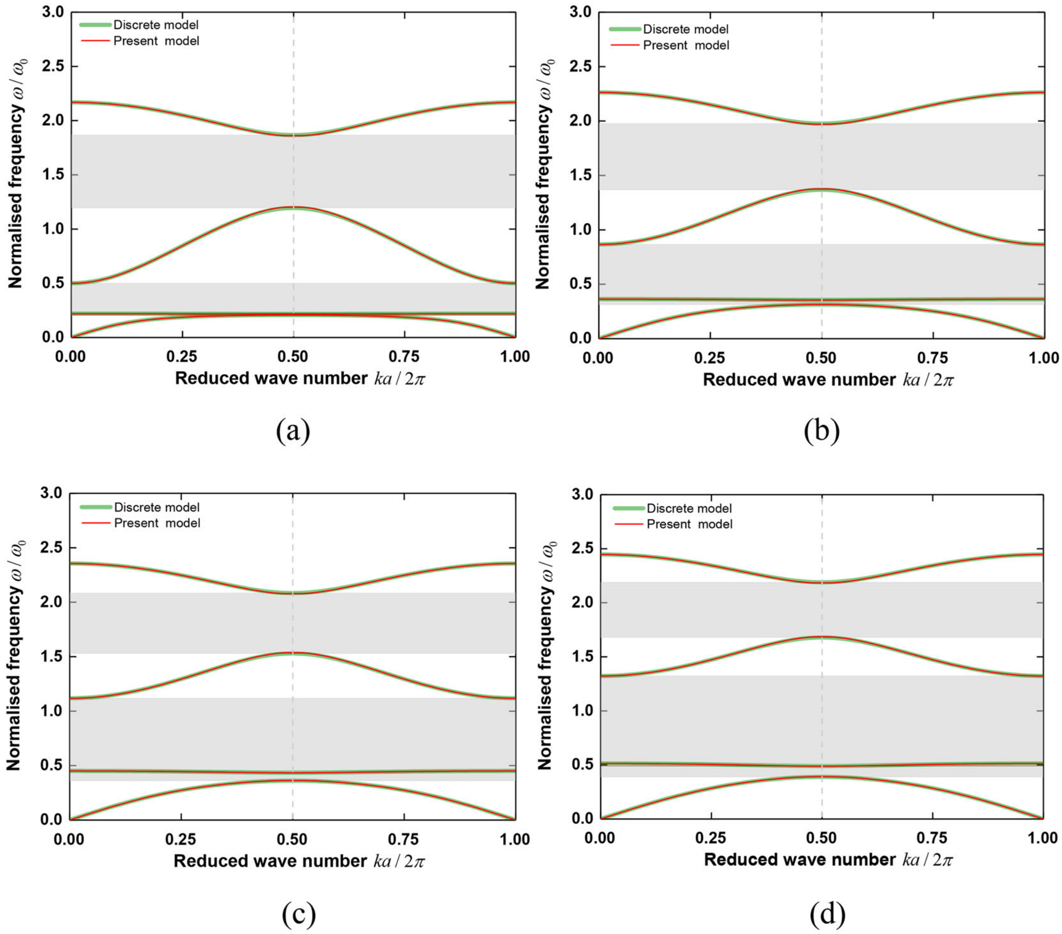


**Figure 7.** Dispersion curves of the discrete and present SG models when $\frac{K_2}{K_1} = \frac{K_2'}{K_1'}$ is set as (a) 1; (b) 3; (c) 5 and (d) 7. For all cases, $\frac{M_2}{M_1} = \frac{m_2}{m_1} = 4$, $\frac{\Delta}{\ell} = 0.1$, $\frac{M_1}{m_1} = 2$ and $\frac{K_1'}{K_1} = 0.5$.

band gap decreases. For a fixed $\frac{\Delta}{\ell}$, the first band gap becomes narrower as $\alpha$ increase whereas the third one becomes wider. The variation of the second one is more complex. It can also be found that the second band gap width varies in a larger parameter space than those of the first and third gaps. Additionally, when selecting certain $\alpha$ and $\frac{\Delta}{\ell}$, we can make the values of band widths approach to zeros which indicate that the corresponding band gaps disappear.

- Figure 10(a,c,e) depicts the variation of lower bounds of three band gaps with stiffness and prestress parameters. When $\frac{\Delta}{\ell}$ fixed, the values of three lower bounds increase with the increase in $\beta$. Similarly, when $\beta$ fixed, the values of three lower bounds increase with the increase in $\frac{\Delta}{\ell}$. Therefore, when both parameters $\beta$ and $\frac{\Delta}{\ell}$ are taken as the larger values, a maximum point of the lower bound can be formed.
- Figure 10(b,d,f) illustrates how three band gap widths change with $\beta$ and $\frac{\Delta}{\ell}$. The first and second band gaps are widened with the increase in $\beta$ or $\frac{\Delta}{\ell}$ whereas the third one is narrowed. In the given parameter space, the change of the first band width is weaker and often tends to zero. Comparatively, two parameters have larger effects on the second band gap and the variation of corresponding value is more obvious. Based on this, the maximal width of each band gap can be obtained by selecting appreciate parameters $\beta$ and $\frac{\Delta}{\ell}$.

Consequently, adjusting mass, stiffness and prestress parameters are helpful to control changes of frequency level and width of each band gap. The higher frequency band gaps tend to appear in PDL with a lower mass ratio, a higher stiffness ratio and a larger prestress parameter. The existence of prestress also provides more parameter choices for band gap design. Based on the above analysis, choosing a reasonable parameter space is conducive to achieving elastic wave control and promoting band gap design.

## 6. Influences of orders of SG continua: 1D diatomic chain with local interactions as an example

Although it is generally believed that the SG continuum with higher SG orders can show higher accuracy, determining which SG order we can adopt to adequately capture satisfactory band gap characteristics is still necessary. In this section, we compare the dispersion curves of the proposed continuum model with different orders to obtain more accurate results. Different from the existing continua, the present model is modified by adopting wavelength-dependent Taylor expansion. Four continua are examined, i.e., fifth-, sixth-, eighth- and tenth-order ones.

Dispersion curves of the present and the discrete models are shown in Figure 11. According to Figure 11(a–d), it is obvious that the proposed SG continuum in which the

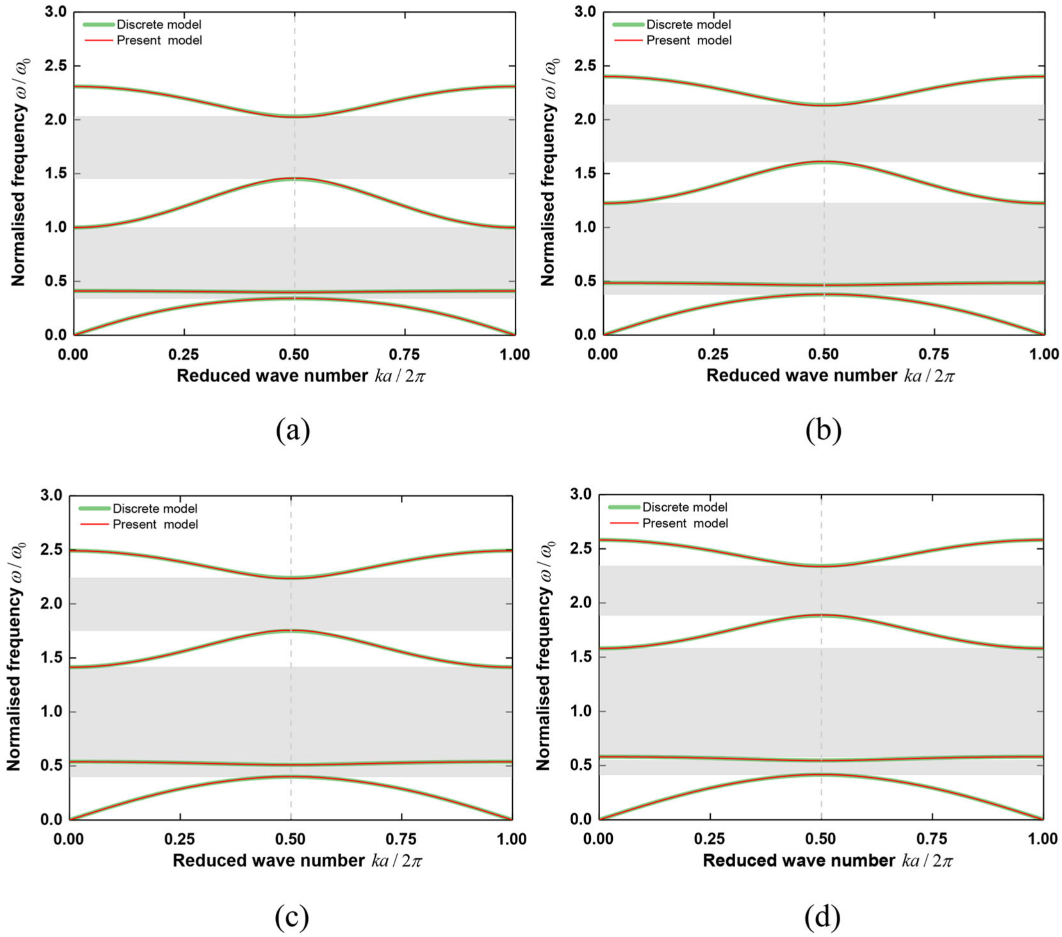


**Figure 8.** Dispersion curves of the discrete and present SG models when $\frac{\Delta}{\ell}$ is set as (a) 0.2; (b) 0.3; (c) 0.4 and (d) 0.5. For all cases, $\frac{M_2}{M_1} = \frac{m_2}{m_1} = 4$, $\frac{K_2}{K_1} = \frac{K_2'}{K_1'} = 2$, $\frac{M_1}{m_1} = 2$ and $\frac{K_1'}{K_1} = 0.5$.

wavelength dependent Taylor expansion is employed can effectively predict the dispersion behavior of discrete model and the accuracy of prediction is also improved as SG orders increase. The curves of fifth- and sixth- order continua are basically consistent with those for the discrete model, except when wave number $\frac{ka}{2\pi}$ is around 0.5. The difference between continuum and discrete models can be explained as follows. According to Eq. (27), the maximum of $d_I$ namely $d_I^{\max}$ is equal to $a$. The Taylor expansion becomes the most inaccurate around $\frac{ka}{2\pi} = 0.5$, attributing to the presence of the maximum of $d_I$, i.e., the distance between $x + a$ and the reference position is the maximum among all wavelengths at that moment. However, increasing SG orders can easily overcome this problem. For example, when orders rise to 8 or 10, the bias can be eliminated and dispersive diagrams of the present model keep a much better consistency with those of discrete model in the whole first Brillouin zone. Therefore, the eighth-order SG continuum is mainly adopted.

## 7. Lattices with different nonlocal interactions

For general lattice metamaterials, only local interactions between two adjacent particles are taken into consideration. In this section, we introduce complex nonlocal interactions and derive SG continuum model for the corresponding PDL. Efforts are devoted to analyzing the impact of local and nonlocal interactions on band gap properties. Lattice with up to two- and three-neighbor interactions are investigated.

The dispersive relationship of the discrete model with up to two-neighbor interactions has already been derived in Section 2, i.e., Eq. (14) and there is no more explanation here. To discuss the effects of two-neighbor interactions, we adopt the unit cell as shown in Figure 1(c) to develop SG continuum model for PDL. The chosen unit cell is composed of the whole mass particles $M_1$ and $M_2$, two half mass particles $m_1$ and $m_2$, two whole internal springs $K_2$ connecting $M_1$ and $M_2$, four half internal springs $K_2'$ connecting $m_1$ and $m_2$, two one-neighbor springs $K_1$ and $K_1'$ connecting $M_1$ and $m_1$, two half two-neighbor springs $K_3$ connecting $M_1$ and one two-neighbor spring $K_3'$ connecting $m_1$.

The kinetic and potential energy densities can be expressed as, respectively

$$T = \frac{1}{2Aa}\left[M_1\left(\dot{u}_1^{(2n)}\right)^2 + M_2\left(\dot{u}_2^{(2n)}\right)^2 + \frac{m_1}{2}\left(\dot{u}_1^{(2n+1)}\right)^2 + \frac{m_1}{2}\left(\dot{u}_1^{(2n-1)}\right)^2 + \frac{m_2}{2}\left(\dot{u}_2^{(2n+1)}\right)^2 + \frac{m_2}{2}\left(\dot{u}_2^{(2n-1)}\right)^2\right] \tag{46}$$

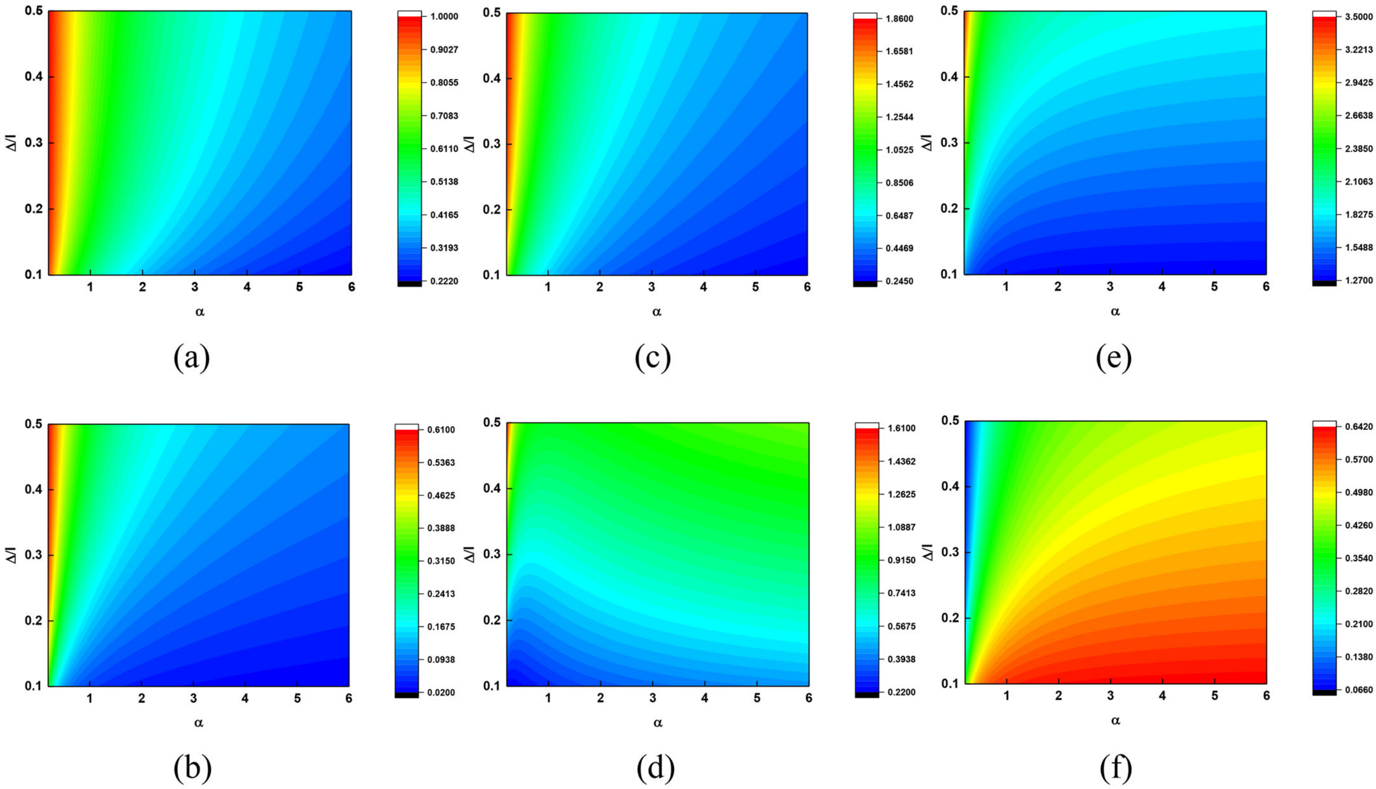


**Figure 9.** Variations of lower bounds and band widths of band gaps with mass and prestress parameters, i.e., $\alpha = \frac{M_2}{M_1} = \frac{m_2}{m_1}$ and $\frac{\Delta}{\ell}$ : (a), (b) the first band gap; (c), (d) the second band gap; (e), (f) the third band gap.

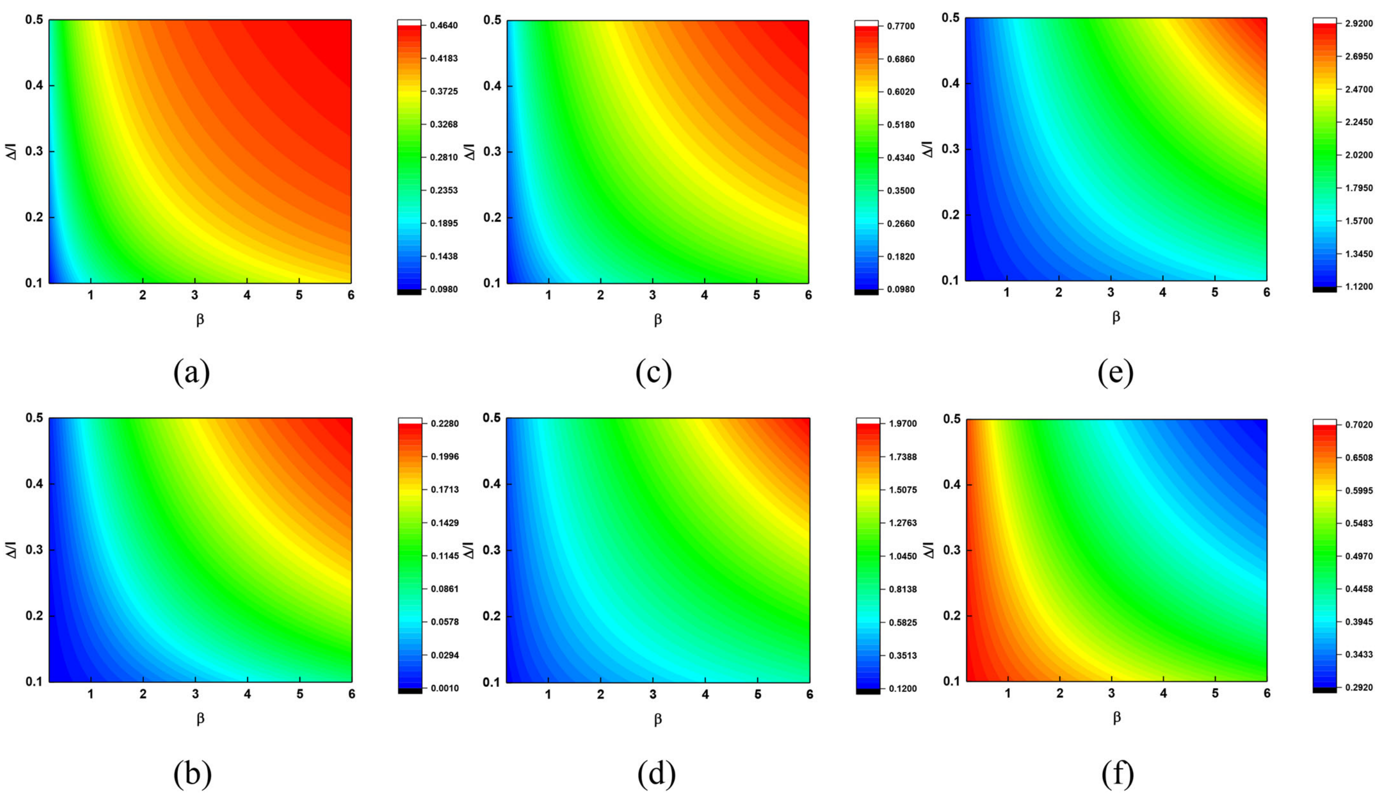


**Figure 10.** Variations of lower bounds and band widths of band gaps with spring and prestress parameters, i.e., $\beta = \frac{K_2}{K_1} = \frac{K_2'}{K_1'}$ and $\frac{\Delta}{\ell}$ : (a), (b) the first band gap; (c), (d) the second band gap; (e), (f) the third band gap.

$$W=\frac{1}{2Aa}\begin{bmatrix} K_1\left(u_1^{(2n)}-u_1^{(2n-1)}\right)^2+K_1'\left(u_1^{(2n+1)}-u_1^{(2n)}\right)^2 \\ +2\frac{\Delta}{\ell}K_2\left(u_2^{(2n)}-u_1^{(2n)}\right)^2 \\ +\frac{\Delta}{\ell}K_2'\left(u_2^{(2n+1)}-u_1^{(2n+1)}\right)^2 \\ +\frac{\Delta}{\ell}K_2'\left(u_2^{(2n-1)}-u_1^{(2n-1)}\right)^2 \\ +\frac{1}{2}K_3\left(u_1^{(2n)}-u_1^{(2n-2)}\right)^2 \\ +\frac{1}{2}K_3\left(u_1^{(2n+2)}-u_1^{(2n)}\right)^2 \\ +K_3'\left(u_1^{(2n+1)}-u_1^{(2n-1)}\right)^2 \end{bmatrix} \tag{47}$$

$$\begin{vmatrix} \left(\frac{\omega}{\omega_0}\right)^2-2\frac{\Delta}{\ell}\beta-\beta_0-1+\gamma\eta_3 & 2\frac{\Delta}{\ell}\beta & \beta_0+1-\eta_1 & 0 \\ 2\frac{\Delta}{\ell}\beta & \alpha\left(\frac{\omega}{\omega_0}\right)^2-2\frac{\Delta}{\ell}\beta & 0 & 0 \\ 1+\beta_0+\eta_2 & 0 & \frac{1}{\alpha_0}\left(\frac{\omega}{\omega_0}\right)^2-2\frac{\Delta}{\ell}\beta\beta_0-\beta_0-1+\gamma_0\eta_3 & 2\frac{\Delta}{\ell}\beta\beta_0 \\ 0 & 0 & 2\frac{\Delta}{\ell}\beta\beta_0 & \frac{\alpha}{\alpha_0}\left(\frac{\omega}{\omega_0}\right)^2-2\frac{\Delta}{\ell}\beta\beta_0 \end{vmatrix}=0, \tag{48}$$

$$\begin{vmatrix} \begin{matrix}\left(\frac{\omega}{\omega_0}\right)^2-\beta_0-2\frac{\Delta}{\ell}\beta-1\\ -2\gamma+2\gamma\cos(ka)-2\theta\end{matrix} & 2\frac{\Delta}{\ell}\beta & \beta_0+e^{-ika}+\theta e^{ika}+\theta e^{-i2ka} & 0 \\ 2\frac{\Delta}{\ell}\beta & \alpha\left(\frac{\omega}{\omega_0}\right)^2-2\frac{\Delta}{\ell}\beta & 0 & 0 \\ e^{ika}+\beta_0+\theta e^{i2ka}+\theta e^{-ika} & 0 & \begin{matrix}\frac{1}{\alpha_0}\left(\frac{\omega}{\omega_0}\right)^2-\beta_0-1-2\frac{\Delta}{\ell}\beta\beta_0\\ -2\gamma_0+2\gamma_0\cos(ka)-2\theta\end{matrix} & 2\frac{\Delta}{\ell}\beta\beta_0 \\ 0 & 0 & 2\frac{\Delta}{\ell}\beta\beta_0 & \frac{\alpha}{\alpha_0}\left(\frac{\omega}{\omega_0}\right)^2-2\frac{\Delta}{\ell}\beta\beta_0 \end{vmatrix}=0 \tag{49}$$

$$\begin{vmatrix} \begin{matrix}\left(\frac{\omega}{\omega_0}\right)^2-2\frac{\Delta}{\ell}\beta-\beta_0\\ -1-2\theta+\gamma\eta_3\end{matrix} & 2\frac{\Delta}{\ell}\beta & \beta_0+1+2\theta-\eta_1+\theta\eta_2-\theta\eta_4 & 0 \\ 2\frac{\Delta}{\ell}\beta & \alpha\left(\frac{\omega}{\omega_0}\right)^2-2\frac{\Delta}{\ell}\beta & 0 & 0 \\ 1+\beta_0+2\theta+\eta_2-\theta\eta_1+\theta\eta_5 & 0 & \begin{matrix}\frac{1}{\alpha_0}\left(\frac{\omega}{\omega_0}\right)^2-2\frac{\Delta}{\ell}\beta\beta_0\\ -\beta_0-1-2\theta+\gamma_0\eta_3\end{matrix} & 2\frac{\Delta}{\ell}\beta\beta_0 \\ 0 & 0 & 2\frac{\Delta}{\ell}\beta\beta_0 & \frac{\alpha}{\alpha_0}\left(\frac{\omega}{\omega_0}\right)^2-2\frac{\Delta}{\ell}\beta\beta_0 \end{vmatrix}=0. \tag{50}$$

Referencing to the procedure in Section 3 and setting dimensionless parameters, we can obtain the corresponding EOMs and dispersive relation.

Equation (48) is the dispersive equation of the proposed continuum model, where $\eta_3=(ikd_I)^2+\frac{(ikd_I)^4}{12}+\frac{(ikd_I)^6}{360}+\frac{(ikd_I)^8}{20160}$ and the value of $d_I$ is determined by Eq. (27).

The nonlocal interactions greatly influence the band gap structure of PDL. The specific dispersion diagrams are shown in Figure 2(b). The dispersion curves of the present model still agree well with those of the discrete model in the whole Brillouin zone, suggesting that the proposed continuum model can be used to predict bandgap characteristics of PDL with complex neighboring interactions. Different from band gap distribution of PDL only with one-neighbor interactions, the first and third band gaps disappear, whereas the second one exists in low-frequency range and is narrowed. The shape and position of dispersion curves also change significantly. For example, the acoustic and optical branches locate at the low-frequency region and the fourth one becomes convex.

The addition of nonlocal interactions and prestress broadens the space for designing expected band gaps. Figure 12 depicts the variation of lower bound and width of each band gap as the function of stiffness ratio $\gamma$ and prestress parameter $\frac{\Delta}{\ell}$. All the values of three lower bounds gradually increase with the increase in parameter $\frac{\Delta}{\ell}$ when $\gamma$ is fixed. When making the value of $\frac{\Delta}{\ell}$ constant, the first two lower bounds slightly change with the increase of $\gamma$, whereas the growth rate of the third one is relatively large, and the maximum value emerges when the values of $\frac{\Delta}{\ell}$ and $\gamma$ are higher. As shown in Figure 12(d), as $\frac{\Delta}{\ell}$ deceases or increases, the trend of the second band width variation resembles that of its lower bound variation and the value of width is always less than 1. When $\gamma>1$, the other two band widths values are still equal to zero no matter how $\frac{\Delta}{\ell}$

changes, indicating the absence of gaps. Furthermore, within the selected parameter range, the first band width is affected slightly and its value is close to zero.

Figure 13 shows the changes of lower bounds and band widths of band gaps with stiffness ratio $\gamma_0$ and prestress parameter $\frac{\Delta}{\ell}$. Three lower bounds increase or decrease as $\frac{\Delta}{\ell}$ and $\gamma_0$ alter and the variation tendency is similar to that in Figure 12(a,c,e). Apparently, the first and third band widths do not any change and the values are always equal to zeros. The second one changes significantly with the increase in $\frac{\Delta}{\ell}$, whereas the effect of $\gamma_0$ is rather weak. We can set optimal $\frac{\Delta}{\ell}$, $\gamma$ and $\gamma_0$ to seek the maximum of band gap width. As a whole, the nonlocal interactions have a great significance on PDL band structures.

We further investigate the lattice with up to three-neighbor interactions to illustrate the effects of nonlocal interactions on band gap properties of PDL. Following the derivation procedure in Section 2, the dispersive equation of the discrete model can be written as

where $K_4$ represents the third nearest neighboring interactions and the parameter $\theta = \frac{K_4}{K_1}$ is set.

Similarly, choosing the unit cell in Figure 1(d) and referring to derivation procedure given in Section 3, we can get the dispersive equation of the corresponding continuum model, that is

where $\eta_4 = \sum_{p=1}^{8} (-1)^{p+1}\frac{(ikd_{II})^p}{p!}$, $\eta_5 = \sum_{p=1}^{8} \frac{(ikd_{II})^p}{p!}$ and the values of $d_I$ and $d_{II}$ are determined by the modified wavelength rule, as shown below.

From Figure 4(b), the wavelength rule is modified and expressed as

$$\text{when } \lambda \in \left[a, \tfrac{4a}{3}\right],\ d_I = a - \lambda, d_{II} = 2(a - \lambda); \tag{51}$$

$$\text{when } \lambda \in \left(\tfrac{4a}{3}, 2a\right],\ d_I = a - \lambda, d_{II} = 2a - \lambda; \tag{52}$$

$$\text{when } \lambda \in (2a, 4a],\ d_I = a, d_{II} = 2a - \lambda; \tag{53}$$

$$\text{when } \lambda \in (4a, +\infty),\ d_I = a, d_{II} = 2a. \tag{54}$$

The practicable range of the long-wave approximation is further narrowed due to the addition of three-neighbor interactions. Moreover, the dispersion curves become more complex, meaning that more local stationary values exist, as presented in Figure 2(c). In the whole first Brillouin zone, the present SG continuum model can well capture the ups and downs in the dispersion curve, when the wavelength-dependent Taylor expansion is adopted. Due to the influence of three-neighbor interactions, only two band gaps exist. One is relatively narrower and appears in the higher frequency region, whereas the other one is much wider and appears in the lower frequency region. Besides this, the shapes of the third and fourth branches curve changes significantly, becoming flatter. The performance of the proposed SG continua for doing with the 1D periodic structure with local/nonlocal interactions is appreciable.

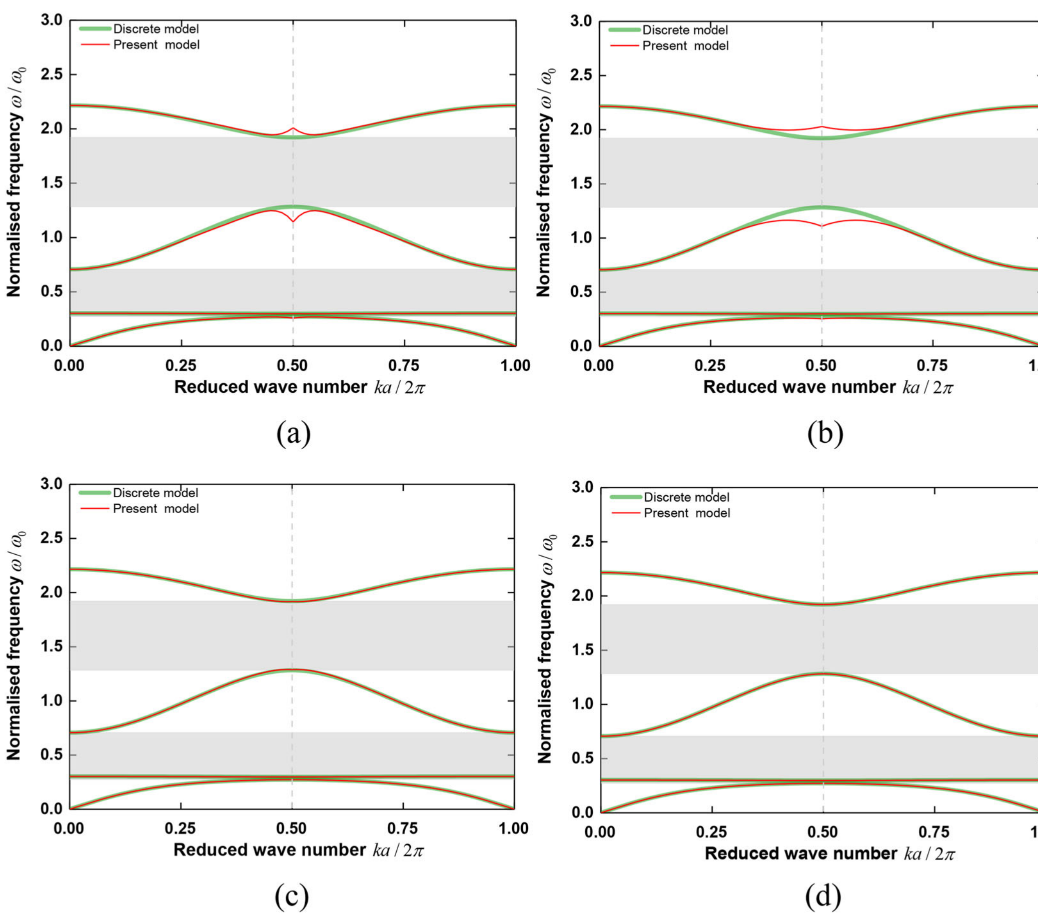


**Figure 11.** Dispersion curves of the present and the discrete models (a) The fifth-order truncation; (b) The sixth-order truncation; (c) The eighth-order truncation; (d) The tenth-order truncation. For all cases, $\frac{M_2}{M_1} = \frac{m_2}{m_1} = 4$, $\frac{K_2}{K_1} = \frac{K_2'}{K_1'} = 2$, $\frac{M_1}{m_1} = 2$, $\frac{K_1'}{K_1} = 0.5$ and $\frac{\Delta}{\ell} = 0.1$.

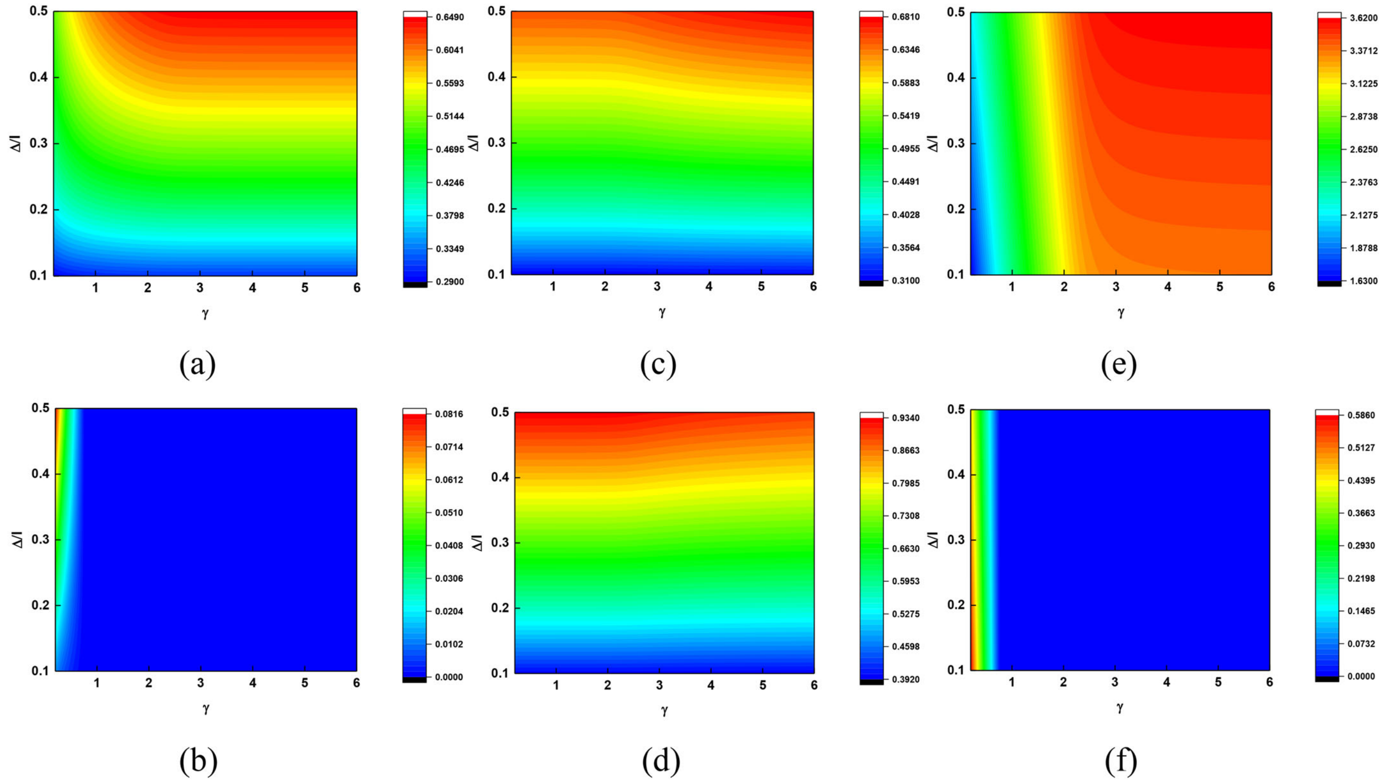


**Figure 12.** Variations of lower bounds and band widths of band gaps with stiffness ratio and prestress parameter, i.e., $\gamma = \frac{K_3}{K_1}$ and $\frac{\Delta}{\ell}$ : (a), (b) the first band gap; (c), (d) the second band gap; (e), (f) the third band gap.

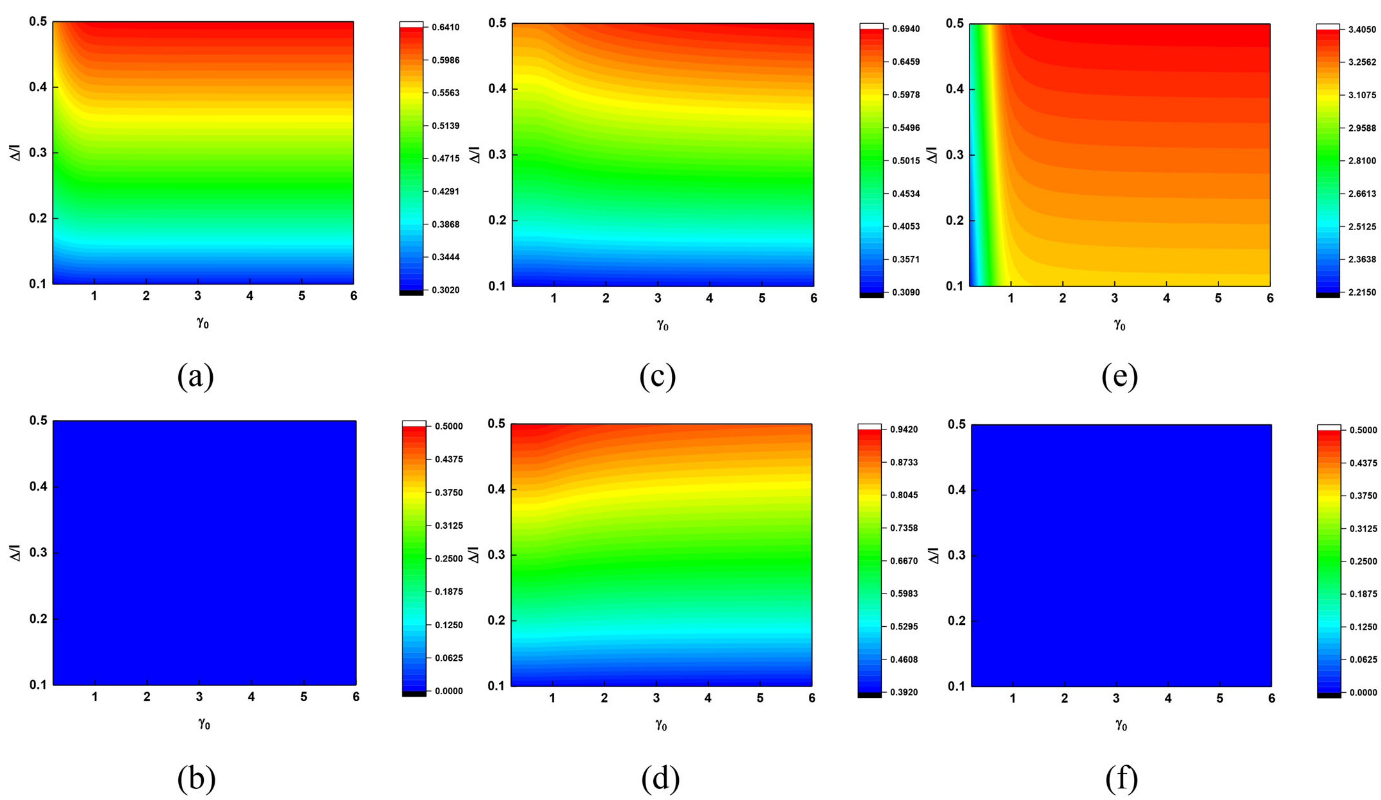


**Figure 13.** Variations of lower bounds and band widths of band gaps with stiffness ratio and prestress parameter, i.e., $\gamma_0 = \frac{K_3'}{K_1}$ and $\frac{\Delta}{\ell}$ : (a), (b) the first band gap; (c), (d) the second band gap; (e), (f) the third band gap.

## 8. Conclusions

The exact strain gradient model of PDL has been mainly supported by modifying the Taylor expansion of displacements. With the wavelength-dependent Taylor expansion adopted, the present model successfully predicts the dispersion curves throughout the first Brillouin zone, suggesting a substantial improvement compared with conventional continuum theories. To the best knowledge of the author, the present model is among the first to successfully predict the bandgap characteristics of PDL.

In this work, a modified lattice system where internal springs are initially elongated has been presented. The corresponding continuum model has also been proposed. Based on this, some relative problems, that is, the effects of mass and stiffness ratios, prestress parameter, orders of SG continua and local/nonlocal interactions have been discussed. The main findings are as follows. (1) The presence of prestress parameter provides a new approach for band gap modulation. Through the adjustment of multiple influencing factors, the intended band gaps can be obtained and the SG continua can still show robust ability to capture band gap properties of PDL. (2) The analysis reveals that only increasing the truncation orders cannot essentially improve the performance of the proposed continuum model, but modifying the Taylor expansion of displacement fields can do this. Once the wavelength-dependent Taylor expansion is adopted, the accuracy of results achieved from the present model is enhanced as higher-order terms added. In this study, it can be found that the eighth-order truncation is enough feasible. (3) Also, it can be demonstrated that the inclusion of nonlocal interactions increases local extremum in the dispersion curves and narrows the workable range of long-wave approximation, making models more complicated. The band gap structures are greatly affected by nonlocal interactions. It is of significance to select the proper unit cell to ensure the acquisition of effective prediction.

Although the 1D case has been discussed here, the proposed methodology is also helpful to investigate features of wave propagations in plane and bulk media with periodic microstructures. In this work, only linear case has been investigated.

## Nomenclature

| | |
|---|---|
| $M_1$ | outer mass located at $\ldots 2n-2, 2n, 2n+2\ldots$ |
| $M_2$ | inner mass located at $\ldots 2n-2, 2n, 2n+2\ldots$ |
| $m_1$ | outer mass located at $\ldots 2n-1, 2n+1, 2n+3\ldots$ |
| $m_2$ | inner mass located at $\ldots 2n-1, 2n+1, 2n+3\ldots$ |
| $K_1$ | stiffness of one-neighbor spring connecting $m_1$ and $M_1$ |
| $K_1'$ | stiffness of one-neighbor spring connecting $M_1$ and $m_1$ |
| $K_2$ | stiffness of internal spring connecting $M_1$ and $M_2$ |
| $K_2'$ | stiffness of internal spring connecting $m_1$ and $m_2$ |
| $K_3$ | stiffness of two-neighbor spring connecting $M_1$ and next $M_1$ |
| $K_3'$ | stiffness of two-neighbor spring connecting $m_1$ and next $m_1$ |
| $K_4$ | stiffness of three-neighbor spring connecting $M_1$ and $m_1$ |
| $\omega_0$ | natural frequency $\sqrt{\frac{K_1}{M_1}}$ |
| $j$ | position parameter $(j = \ldots 2n-2, 2n-1, 2n, 2n+1, 2n+2\ldots)$ |
| $u_1^{(j)}$ | displacement of outer mass located at $j$ |
| $u_2^{(j)}$ | displacement of inner mass located at $j$ |
| $A_1$ | amplitude of the displacement $u_1^{(j)}$ $(j = \ldots 2n-2, 2n, 2n+2\ldots)$ |
| $A_2$ | amplitude of the displacement $u_2^{(j)}$ $(j = \ldots 2n-2, 2n, 2n+2\ldots)$ |
| $B_1$ | amplitude of the displacement $u_1^{(j)}$ $(j = \ldots 2n-1, 2n+1, 2n+3\ldots)$ |
| $B_2$ | amplitude of the displacement $u_2^{(j)}$ $(j = \ldots 2n-1, 2n+1, 2n+3\ldots)$ |
| $\alpha$ | mass ratio $\frac{M_2}{M_1}$ and $\frac{m_2}{m_1}$ |
| $\alpha_0$ | mass ratio $\frac{M_1}{m_1}$ |
| $\beta$ | stiffness ratio $\frac{K_2}{K_1}$ and $\frac{K_2'}{K_1'}$ |
| $\beta_0$ | stiffness ratio $\frac{K_1'}{K_1}$ |
| $\gamma$ | stiffness ratio $\frac{K_3}{K_1}$ |
| $\gamma_0$ | stiffness ratio $\frac{K_3'}{K_1}$ |
| $\theta$ | stiffness ratio $\frac{K_4}{K_1}$ |
| $\xi$ | original length of internal spring |
| $\ell$ | length after deformation of internal spring |
| $u_1(x,t)$ | continuous displacement field of mass $M_1$ |
| $\tilde{u}_1(x,t)$ | continuous displacement field of mass $M_2$ |
| $u_2(x,t)$ | continuous displacement field of mass $m_1$ |
| $\tilde{u}_2(x,t)$ | continuous displacement field of mass $m_2$ |
| $C_1$ | amplitude of continuous displacement field $u_1(x,t)$ |
| $C_2$ | amplitude of continuous displacement field $\tilde{u}_1(x,t)$ |
| $D_1$ | amplitude of continuous displacement field $u_2(x,t)$ |
| $D_2$ | amplitude of continuous displacement field $\tilde{u}_2(x,t)$ |
| $\Delta$ | initial elongation $\gg u_2^{(j)} - u_1^{(j)}$ |
| $d_I$ | the first wavelength-dependent correction |
| $d_{II}$ | the second wavelength-dependent correction |
| $a$ | lattice spacing |
| $Aa$ | volume of the unit cell |
| $l$ | arbitrary integer |
| $n$ | arbitrary integer |
| $\lambda$ | wavelength |
| $p$ | any positive integer |
| $\omega$ | angular frequency |
| $k$ | wave number |
| $T$ | kinetic energy density |
| $W$ | potential energy density |
| $\eta_1$ | wavelength-dependent Taylor expansion $\sum_{p=1}^{8}(-1)^{p+1}\frac{(ikd_I)^p}{p!}$ |
| $\eta_2$ | wavelength-dependent Taylor expansion $\sum_{p=1}^{8}\frac{(ikd_I)^p}{p!}$ |
| $\eta_1^+$ | wavelength-dependent Taylor expansion $\sum_{p=1}^{10}(-1)^{p+1}\frac{(ikd_I)^p}{p!}$ |
| $\eta_2^+$ | wavelength-dependent Taylor expansion $\sum_{p=1}^{10}\frac{(ikd_I)^p}{p!}$ |
| $\eta_3$ | wavelength-dependent Taylor expansion $(ikd_I)^2 + \frac{(ikd_I)^4}{12} + \frac{(ikd_I)^6}{360} + \frac{(ikd_I)^8}{20160}$ |
| $\eta_4$ | wavelength-dependent Taylor expansion $\sum_{p=1}^{8}(-1)^{p+1}\frac{(ikd_{II})^p}{p!}$ |
| $\eta_5$ | wavelength-dependent Taylor expansion $\sum_{p=1}^{8}\frac{(ikd_{II})^p}{p!}$ |

## Acknowledgments

The authors are grateful for the helpful comments from reviewers.

## Funding

The work was supported by the National Natural Science Foundation of China (Grant No. 11972174 and Grant No. 11672119).

## References

[1] G. Singh, R. Ni, and A. Marwaha, A review of metamaterials and its applications, Int. J. Eng. Trend. Technol., vol. 19, no. 6, pp. 305–310, 2015. DOI: 10.14445/22315381/IJETT-V19P254.

[2] A. Valipour, M.H. Kargozarfard, M. Rakhshi, A. Yaghootian, and H.M. Sedighi, Metamaterials and their applications: an

overview, Proc. Inst. Mech Eng. Part L. J. Mater. Design Appl., vol. 0, pp. 1–40, 2021.

[3] L. Fok, M. Ambati, and X. Zhang, Acoustic metamaterials, MRS Bull., vol. 33, no. 10, pp. 931–934, 2008. DOI: 10.1557/mrs2008.202.

[4] J.Y. Liu, H.B. Guo, and T. Wang, A review of acoustic metamaterials and phononic crystals, Crystals, vol. 10, no. 4, pp. 1–26, 2020. DOI: 10.3390/cryst10040305.

[5] X. Fang, J.H. Wen, B. Bonello, J.F. Yin, and D.L. Yu, Wave propagation in one-dimensional nonlinear acoustic metamaterials, New J. Phys., vol. 19, no. 5, pp. 053007, 2017. DOI: 10.1088/1367-2630/aa6d49.

[6] H.H. Huang, and C.T. Sun, Anomalous wave propagation in a one-dimensional acoustic metamaterial having simultaneously negative mass density and Young's modulus, J. Acoust. Soc. Am., vol. 132, no. 4, pp. 2887–2895, 2012. DOI: 10.1121/1.4744977.

[7] H.H. Huang, and C.T. Sun, Wave attenuation mechanism in an acoustic metamaterial with negative effective mass density, New J. Phys., vol. 11, no. 1, pp. 013003, 2009. DOI: 10.1088/1367-2630/11/1/013003.

[8] H.H. Huang, C.T. Sun, and G.L. Huang, On the negative effective mass density in acoustic metamaterials, Int. J. Eng. Sci., vol. 47, no. 4, pp. 610–617, 2009. DOI: 10.1016/j.ijengsci.2008.12.007.

[9] R. Khajehtourian, and M.I. Hussein, Dispersion characteristics of a nonlinear elastic metamaterial, AIP Adv., vol. 4, no. 12, pp. 124308, 2014. DOI: 10.1063/1.4905051.

[10] P.P. Kulkarni, and J.M. Manimala, Longitudinal elastic wave propagation characteristics of inertant acoustic metamaterials, J. Appl. Phys., vol. 119, no. 24, pp. 245101, 2016. DOI: 10.1063/1.4954074.

[11] J. Li, and C.T. Chan, Double-negative acoustic metamaterial, Phys. Rev. E., vol. 70, no. 5, pp. 055602, 2004.

[12] S.S. Yao, X.M. Zhou, and G.K. Hu, Experimental study on negative effective mass in a 1D mass–spring system, New J. Phys., vol. 10, no. 4, pp. 043020, 2008. DOI: 10.1088/1367-2630/10/4/043020.

[13] I.L. Chang, Z.X. Liang, H.W. Kao, S.H. Chang, and C.Y. Yang, The wave attenuation mechanism of the periodic local resonant metamaterial, J. Sound Vib., vol. 412, pp. 349–359, 2018. DOI: 10.1016/j.jsv.2017.10.008.

[14] X.F. Lei, H.P. Hou, P. Liu, Z.F. Xu, S.H. Liu, and B.B. Hu, Flexural vibration band gaps in Bragg acoustical hyperstructure beam with local-resonance system, Mod. Phys. Lett. B., vol. 33, no. 23, pp. 1950278, 2019. DOI: 10.1142/S0217984919502786.

[15] G.B. Hu, L.H. Tang, R. Das, S.Q. Gao, and H.P. Liu, Acoustic metamaterials with coupled local resonators for broadband vibration suppression, AIP Adv., vol. 7, no. 2, pp. 025211, 2017. DOI: 10.1063/1.4977559.

[16] P.C. Zhao, K. Zhang, C. Zhao, and Z.C. Deng, Multi-resonator coupled metamaterials for broadband vibration suppression, Appl. Math. Mech-Engl. Ed., vol. 42, no. 1, pp. 53–64, 2021. DOI: 10.1007/s10483-021-2684-8.

[17] K.T. Tan, H.H. Huang, and C.T. Sun, Optimizing the band gap of effective mass negativity in acoustic metamaterials, Appl. Phys. Lett., vol. 101, no. 24, pp. 241902, 2012. DOI: 10.1063/1.4770370.

[18] Y.L. Li, X.N. Wang, and G.W. Yan, Configuration effect and bandgap mechanism of quasi-one-dimensional periodic lattice structure, Int. J. Mech. Sci., vol. 190, pp. 106017, 2021. DOI: 10.1016/j.ijmecsci.2020.106017.

[19] X.Q. Zhou, J. Wang, R.Q. Wang, and J.Q. Lin, Effects of relevant parameters on the bandgaps of acoustic metamaterials with multi-resonators, Appl. Phys. A., vol. 122, no. 4, pp. 1–8, 2016.

[20] C.C. Liu, and C. Reina, Broadband locally resonant metamaterials with graded hierarchical architecture, J. Appl. Phys., vol. 123, no. 9, pp. 095108, 2018. DOI: 10.1063/1.5003264.

[21] Y.H. Zhou, P.J. Wei, Y.Q. Li, and Q.H. Tang, Continuum model of acoustic metamaterials with diatomic crystal lattice, Mech. Adv. Mater. Struct., vol. 24, no. 13, pp. 1059–1073, 2017. DOI: 10.1080/15376494.2016.1205685.

[22] R.D. Mindlin, Second gradient of strain and surface-tension in linear elasticity, Int. J. Solids Struct., vol. 1, no. 4, pp. 417–438, 1965. DOI: 10.1016/0020-7683(65)90006-5.

[23] D. Polyzos, and D.I. Fotiadis, Derivation of Mindlin's first and second strain gradient elastic theory via simple lattice and continuum models, Int. J. Solids Struct., vol. 49, no. 3–4, pp. 470–480, 2012. DOI: 10.1016/j.ijsolstr.2011.10.021.

[24] D. De Domenico, H. Askes, and E.C. Aifantis, Discussion of "Derivation of Mindlin's first and second strain gradient elastic theory via simple lattice and continuum models" by Polyzos and Fotiadis, Int. J. Solids Struct., vol. 191–192, pp. 646–651, 2020. DOI: 10.1016/j.ijsolstr.2019.11.016.

[25] R. Zhu, H.H. Huang, G.L. Huang, and C.T. Sun, Microstructure continuum modeling of an elastic metamaterial, Int. J. Eng. Sci., vol. 49, no. 12, pp. 1477–1485, 2011. DOI: 10.1016/j.ijengsci.2011.04.005.

[26] Y.H. Zhou, P.J. Wei, and Q.H. Tang, Continuum model of a one-dimensional lattice of metamaterials, Acta Mech., vol. 227, no. 8, pp. 2361–2376, 2016. DOI: 10.1007/s00707-016-1613-6.

[27] Y.H. Zhou, P.J. Wei, Y.Q. Li, and L. Li, Continuum model of two-dimensional crystal lattice of metamaterials, Mech. Adv. Mater. Struct., vol. 26, no. 3, pp. 224–237, 2019. DOI: 10.1080/15376494.2017.1341582.

[28] D. Bigoni, M. Gei, and A.B. Movchan, Dynamics of a prestressed stiff layer on an elastic half space: filtering and band gap characteristics of periodic structural models derived from long-wave asymptotics, J. Mech. Phys. Solids., vol. 56, no. 7, pp. 2494–2520, 2008. DOI: 10.1016/j.jmps.2008.02.007.

[29] A. Amendola, A. Krushynska, C. Daraio, N.M. Pugno, and F. Fraternali, Tuning frequency band gaps of tensegrity mass-spring chains with local and global prestress, Int. J. Solids Struct., vol. 155, pp. 47–56, 2018. DOI: 10.1016/j.ijsolstr.2018.07.002.

[30] M. Miniaci, M. Mazzotti, A. Amendola, and F. Fraternali, Effect of prestress on phononic band gaps induced by inertial amplification, Int. J. Solids Struct., vol. 216, pp. 156–166, 2021. DOI: 10.1016/j.ijsolstr.2020.12.011.

[31] R.X. Feng, and K.X. Liu, Tuning of band-gap of phononic crystals with initial confining pressure, Chin. Phys. B., vol. 21, no. 12, pp. 126301, 2012. DOI: 10.1088/1674-1056/21/12/126301.

[32] R.X. Feng, and K.X. Liu, Tuning the band-gap of phononic crystals with an initial stress, Physica B., vol. 407, no. 12, pp. 2032–2036, 2012. DOI: 10.1016/j.physb.2012.01.135.

[33] N. Challamel, H. Zhang, C.M. Wang, and J. Kaplunov, Scale effect and higher-order boundary conditions for generalized lattices, with direct and indirect interactions, Mech. Res. Commun., vol. 97, pp. 1–7, 2019. DOI: 10.1016/j.mechrescom.2019.04.002.

[34] N. Challamel, C.M. Wang, H. Zhang, and S. Kitipornchai, Exact and nonlocal solutions for vibration of axial lattice with direct and indirect neighboring interactions, J. Eng. Mech., vol. 144, no. 5, pp. 04018025, 2018. DOI: 10.1061/(ASCE)EM.1943-7889.0001441.

[35] E. Ghavanloo, and S.A. Fazelzadeh, Wave propagation in one-dimensional infinite acoustic metamaterials with long-range interactions, Acta Mech., vol. 230, no. 12, pp. 4453–4461, 2019. DOI: 10.1007/s00707-019-02514-8.

[36] B.Y. Wang, J.X. Liu, A.K. Soh, and N.G. Liang, On band gaps of nonlocal acoustic lattice metamaterials: a robust strain gradient model, Appl. Math. Mech-Engl. Ed., vol. 43, no. 1, pp. 1–20, 2022. DOI: 10.1007/s10483-021-2795-5.